Influence of Cement Type on Resistance to Organic Acids

Dyer, Thomas

Published in:
Magazine of Concrete Research

DOI:
10.1680/jmacr.16.00271

Publication date:
2017

Document Version
Peer reviewed version

Magazine of Concrete Research

Influence of Cement Type on Resistance to Organic Acids

--Manuscript Draft--

Manuscript Number:	MACR-D-16-00271R1
Full Title:	Influence of Cement Type on Resistance to Organic Acids
Article Type:	Paper- your paper is on materials research
Corresponding Author:	Thomas D Dyer, BSc MSc PhD University of Dundee Dundee, UNITED KINGDOM
Corresponding Author Secondary Information:	
Corresponding Author's Institution:	University of Dundee
Corresponding Author's Secondary Institution:	
First Author:	Thomas D Dyer, BSc MSc PhD
First Author Secondary Information:	
Order of Authors:	Thomas D Dyer, BSc MSc PhD
Order of Authors Secondary Information:	
Abstract:	Resistance to attack by acids is an important characteristic in a number of concrete applications. Deterioration can occur by three mechanisms: acidolysis, complexolysis and precipitation of expansive reaction products. Generally, where acidolysis is the main mechanism, a low calcium cement is likely to impart enhanced resistance. However, where other mechanisms may also be effective, the approach to selecting cements for acid resistance is less clear. This paper examines the effect of four acids on cement pastes made from three different cement types using measurements of mass loss, chemical and mineralogical analysis and micro CT scanning. In addition, geochemical modelling techniques are employed to further explore the role salt precipitation and complexolysis are likely to play.
Funding Information:	

Cherise Lopes-Baker
ICE Publishing
One Great George Street
London
SW1P 3AA, UK

26.09.2016

Dear Cherise

Attached is the revised version of my paper entitled '**Influence of Cement Type on Resistance to Organic Acids**', with modifications in accordance with the reviews comments.

All changes are highlighted. I have also added an additional sentence in the acknowledgements section regarding a database used as part of the research.

Yours Sincerely,

Thomas Dyer

Concrete Technology Unit
Civil Engineering
University of Dundee
Dundee
DD1 4HN

Date: 26.09.2016
Paper Title: Influence of Cement Type on Resistance to Organic Acids

Thomas Dyer*
Lecturer, University of Dundee

*Concrete Technology Unit,
University of Dundee
Dundee, DD1 4HN
UK
Tel: 01382 388 118
e-mail: t.d.dyer@dundee.ac.uk

Number of words: 7299
Number of tables: 13
Number of figures: 19

INFLUENCE OF CEMENT TYPE ON RESISTANCE TO ORGANIC ACIDS

ABSTRACT

Resistance to attack by acids is an important characteristic in a number of concrete applications. Deterioration can occur by three mechanisms: acidolysis, complexolysis and precipitation of expansive reaction products. Generally, where acidolysis is the main mechanism, a low calcium cement is likely to impart enhanced resistance. However, where other mechanisms may also be effective, the approach to selecting cements for acid resistance is less clear. This paper examines the effect of four acids on cement pastes made from three different cement types using measurements of mass loss, chemical and mineralogical analysis and micro CT scanning. In addition, geochemical modelling techniques are employed to further explore the role salt precipitation and complexolysis are likely to play.

KEYWORDS: Durability-related properties; Modelling; Cement paste

INTRODUCTION

The resistance of concrete to attack under acidic conditions is a characteristic which is required in many industrial and agricultural applications. Vulnerability to such forms of attack stems largely from deterioration of the cement matrix, rather than aggregate, although aggregate containing carbonate minerals may also be susceptible.

The basic mechanism of deterioration resulting from acid attack is that of *acidolysis* – elements in the cement hydration products react with the acid leading to their release as ions in solution, leading to loss of solid matter. In the case of Portland cement, acidolysis initially involves the loss of calcium, since portlandite ($Ca(OH)_2$) is solubilised with a relatively small drop in pH from original conditions. AFm and AFt phases dissolve at slightly lower pH values, but this leads to the precipitation of amorphous aluminium and iron hydroxides, which persist until the pore solution becomes relatively acidic. Exposure to acidic solutions also causes *decalcification* of C-S-H gel, ultimately leaving relatively weak silica gel behind.

Where acidolysis is the main deterioration mechanism (such as for hydrochloric or nitric acid) enhanced acid resistance can be imparted by using a cement with a lower calcium content. Such cements include blends of Portland cement with pozzolanic or latent hydraulic materials. For instance, enhanced resistance to hydrochloric acid has been achieved through the combination of fly ash, natural pozzolana, silica fume and corn cob ash with Portland cement (Siad, Mesbah, Khelafi, Kamali-Bernard and Mouli, 2010; Khedr and Abou-Zeid, 1994; Mehta, 1985; Adesanya and Raheem, 2010). It has also been noted that calcium aluminate cements, having a lower calcium content and, in most cases, a complete absence of portlandite, are also highly resistant (Scrivener, Cabiron and Letourneux, 1999).

However, two other mechanisms can be effective during acid attack which make the achievement of resistance to certain acids more challenging. The first of these mechanisms is *complexolysis*, which occurs when acid ions form complexes with metal ions, allowing more of the solid phases to dissolve (Berthelin, 1983). It should be noted that complexolysis is normally only a significant mechanism where metal ions are already in solution as a result of acidolysis (Burgstaller and Schinner, 1993).

The second mechanism occurs where the salts formed between metal ions from the cement and the acidic species are of low solubility and are precipitated from solution. In some cases, this does not have a damaging effect, since precipitation may not disrupt the cement matrix. However, where the salt has a higher molar volume than the hydration products it replaces, precipitation leads to expansion and cracking (Bertron and Duchesne, 2013). The most common example of this type of deterioration is sulfuric acid attack where acidolysis combines with ettringite and gypsum formation, whose damaging expansive effects are well-documented. In the case of sulfuric acid, the incorporation of pozzolanic materials has also usually been found to improve resistance (Chang, Song, Munn and Marosszeky, 2005; Tamimi, 1997; Torii and Kawamura, 1994; Kim, Lee and Moon, 2007; Durning and Hicks, 1991). Moreover, calcium aluminate cement has been shown to have enhanced resistance when exposed to environments where sulfuric acid is formed by biological processes (Scrivener, Cabiron and Letourneux, 1999).

A wide range of organic acids may also be encountered in the built environment, and these too can be extremely damaging, not least because their modes of attack have the potential to include acidolysis, complexolysis and salt precipitation simultaneously.

The role of cement composition with respect to resistance to attack from organic acids has been much less explored. However, it has been established that the use of pozzolanic materials and GGBS can impart enhanced resistance against organic acids including acetic, lactic and formic acid, and that the use of GGBS is also effective (De Belie, Verselder, De Blaere, Van Nieuwenburg and Verschoore, 1996; De Belie, De Coster and Van Nieuwenburg, 1997; Bertron, Duchesne and Escadeillas, 2005; Pavlík and Unčik, 1997; Bertron, Escadeillas and Duchesne, 2004).

This paper examines the influence of cement composition on resistance to acid attack from organic acids selected for their capacity for forming complexes with metal ions present in cementitious materials and / or their potential to precipitate expansive reaction products.

MATERIALS AND METHODS

The study described in this paper involved the exposure of cement paste cylinders to acidic solutions containing four different organic acids. Changes that these cylinders had undergone were then investigated using micro computed tomography, X-ray diffraction and X-ray fluorescence techniques. Additionally, geochemical modelling is used to further understand the deterioration mechanisms.

Acids

Four organic acids were selected for the study. These were lactic, citric and tartaric acids, plus catechol. The chemical formulae, structures and acid dissociation constants (pK_a) of these compounds are presented in Table 1. It should be noted that the pK_a values are presented as stepwise – rather than cumulative – constants. The acids are discussed further below.

Lactic acid

Lactic acid exists as two isomers – the D- and L- forms – with the L- form produced by living organisms. In this study, L-lactic acid was used and so, wherever possible, constants relating to lactic acid have

been obtained for this form. Table 2 gives the stability constant of complexes formed by lactic acid with calcium and aluminium. The molecule contains two –OH groups, but only the carboxylate group normally undergoes deprotonation. However, interaction with some metal ions allows further deprotonation, as evidenced by the existence of the $Al(CH_3COCO_2)(CH_3C(OH)CO_2)$ complex. The complexes formed between lactic acid and calcium and aluminium ions are relatively weak. It is likely that iron also forms complexes with lactic acid, but reliable stability constants have not been reported in the literature (Hamada, Carlson and Dangberg, 2005).

Table 3 give solubility products of calcium, aluminium and iron salts formed with lactic acid, along with molar volumes of salts that are known to form, where data exists. Lactic acid was selected on the grounds that it is likely to cause deterioration principally through acidolysis.

Citric acid

Citric acid forms strong complexes with Ca, Al and Fe ions, and is also capable of forming complexes with silicic acid (H_4SiO_4) (Table 4). It is capable of forming a number of salts with calcium, aluminium and iron (Table 5). Calcium citrate tetrahydrate possesses both a low solubility in water and a high molar volume relative to that of portlandite (33 cm^3/mol). As a result, the deterioration of cement exposed to citric acid results from fragmentation due to precipitation of this salt (Bertron and Duchesne, 2013). The extent to which complexolysis plays a role in deterioration is less clear. Thus, citric acid was selected to examine this aspect.

Tartaric acid

Tartaric acid is a chiral compound, with the levotartaric (L-) form being the naturally occurring form and dextrotartaric acid (D-) and mesotartaric acid produced synthetically. D-tartaric acid was used in the experiments described in this paper. Stability constants are provided in Table 6, whilst solubility products of tartrate salts are provided in Table 7. Of these salts, calcium tartrate tetrahydrate is of most significance since its precipitation yields a layer at the cement surface ascribed as having a protective effect (Bertron and Duchesne, 2013). Tartaric acid was therefore selected for this study to further examine this effect, whilst also examining the effect of complex formation.

Catechol

Catechol is a relatively weak acid, and whilst it can occur in environments such as contaminated soils, it was included in the study because catecholate is a commonly occurring functional group on humic and fulvic acid molecules encountered in soils (Drever and Vance, 1994). Catechol forms strong complexes with aluminium and iron (Table 8). Whilst complex formation with calcium ions has not been conclusively demonstrated, their presence leads to modification of the pK_a of catechol (in stepwise terms: pK_{a1} = 9.04; pK_{a2} = 1.64), indicating that it is likely (Lebedev, Ivanova, Timoshin and Ruuge, 2007). The catecholate ion forms relatively strong complexes with Si. Indeed, of the fulvic and humic acid functional groups, the catecholate group would appear to form the strongest Si complexes (Pokrovski and Schott, 1998).

Two calcium catecholate salts are known to form (Table 9). The solubility products provided are based on measurements conducted be the author, details of which will be published in a forthcoming paper. The salts are relatively insoluble and possess high molar volumes. Thus, catechol was selected on the

grounds its complexing abilities and likely salt precipitation during acid attack. Previous research has shown that catechol and similar hydroxyphenols can cause substantial damage to concrete [39].

Cements

The logic behind the selection of cements was to compare the performance of Portland cement to cements with either a higher SiO_2 content and a higher Al_2O_3 content. Thus, three cements were studied: a 52.5 strength class CEM I Portland cement, a CEM II cement containing 35% siliceous fly ash, and a calcium sulfoaluminate cement to which 2% by mass of anhydrite ($CaSO_4$) had been added. The oxide analyses of the cements are shown in Table 10. Cement containing blastfurnace slag was not examined, on the grounds that its composition occupies a space between Portland cement and fly ash, although it should be stressed that good acid resistance has been obtained with this material.

Preparation of paste specimens

A water / cement ratio of 0.5 was employed for all cement pastes. Distilled water was used as the mix water and mixing was carried out by hand. The pastes were poured into polyethylene cylinders with an internal diameter of 22 mm and height of 70 mm. The cylinders were then vibrated to remove as many air bubbles as possible. The top of the cylinders was then sealed with an air-tight lid and the cylinders left in a 25°C environment for a period of 28 days.

Acid attack experiments

In all cases, 4 litres of 0.1M solution of each acid were prepared using reagent grade compounds and distilled water. The solutions were poured into 5 litre capacity polyethylene tanks and their pH was measured using a hand-held pH meter.

The cement paste cylinders were removed from their moulds and weighed to the nearest 0.01g. A cylinder was placed into each tank such that each cement type was exposed to all acids. The tanks were then sealed with an air-tight lid. Exposure to acids was conducted at a temperature of 25 °C.

At intervals, the tanks were opened, the pH of the solutions measured and the cylinders weighed. These time intervals were initially 24 hours, but longer intervals were adopted at later ages, based on the rate at which the measured characteristics were changing.

The specimens were exposed to the acid solutions for a maximum of 90 days. At the end of the exposure period, the specimens were removed and left to dry in air before being transferred to sealed plastic bags and stored in a desiccator until further analysis was conducted. Analysis took the form of three techniques: micro computed tomography, powder X-ray diffraction and X-ray fluorescence spectrometry. The approach taken for each technique is described below.

Micro computed tomography (µCT)

µCT scans were obtained from the specimens exposed to acid solutions using a Nikon XTH225ST scanner. A tungsten excitation target lens was used, under operating conditions of 115kV and 312µA with a 0.5mm copper filter. The sample was located 150mm away from the X-ray source. Angular

increments of 0.11 ° were used, with 2-frame averaging used to form the images at each increment. In instances where fragile cracked outer layers had formed, specimens were held within the same type of plastic cylinder used for moulding, to limit the extent to which mounting in the machine would cause this surface to break away.

Powder X-ray diffraction

Powder X-ray diffraction followed by Rietveld refinement was used to provide a quantitative estimate of the mineralogical composition of the hydrated cement pastes prior to exposure to acid, and the deteriorated surface material after exposure.

At the end of the initial curing period a cylinder of each cement type was removed from its mould and crushed, initially using a percussion mill and subsequently using a mortar and pestle until a fine powder was obtained. The powdered samples were stored in a desiccator containing silica gel and soda lime for a period of 24 hours. A sub-sample was taken and a 5% (by mass) corundum internal standard was added. Sub-samples with and without the internal standard were analysed using a Siemens D5000 diffractometer using a Cu-kα source at 40 mA 40 kV. Scans were run with angular increments of 0.1 °2θ at a rate of 0.67 °2θ per minute.

Rietveld refinement was conducted on the resulting traces to obtain a quantitative estimate of the phase composition of the hydrated pastes using the MAUD software package (Lutterotti, 2010). In the case of AFm and AFt phases, iron was permitted to substitute for aluminium in the structures. Using the quantitative determination of the internal standard, it was possible to estimate the quantity of amorphous material in the paste, and adjust the quantities of crystalline constituents accordingly.

After the exposure period, the surfaces of each specimen had been noticeably altered. To determine the composition of this altered material, a quantity was removed using a scalpel. In some cases, multiple layers were present. In previous work, researchers were able to remove the layers individually (Bertron and Duchesne, 2013). However, in this study, this proved problematic, and the layers were removed together. The material taken from the altered layers was then ground into a powder using a pestle and mortar and analysed in the same manner as the hydrated cement specimens.

X-ray fluorescence spectrometry

The chemical composition of both the hydrated cement pastes and the altered surface layers obtained for powder X-ray diffraction was also determined using X-ray fluorescence spectrometry. The powders were analysed as pressed pellets using a Panalytical Zetium 2.4W X-ray fluorescence spectrometer.

Geochemical modelling

Geochemical modelling was conducted using the PHREEQC software package (Charlton and Parkhurst 2011; Parkhurst and Appelo, 2013) . The basic configuration of the model developed is shown in Figure 1. It consisted of 102 cells connected in sequence. The first cell represented the tank of acid solution and contained 4 kg of water in which 0.1M of acid was dissolved. The pH of the tank cell was set at that calculated based on the dissociation constants of the acid.

The second cell consisted of a small volume of water (467 mg) with a thickness of 0.1 mm. This cell contained the same concentration of acid as the tank cell. This second cell is referred to in the figure

as the 'water surface layer' and was included to act as a means of modelling any precipitation of salts directly at the cylinder surface. The redox potential (expressed as pE) of the solution in both the tank and the water surface layer was set to 8.451, which is typical of surface or ground water containing dissolved oxygen (Chapman, 1996).

The remaining cells represented the interior porosity of the cement paste, with each cell having a thickness of 0.1 mm and containing 97 mg of water in contact with a mineral assemblage defined using PHREEQC's EQUILIBRIUM_PHASES keyword, with an initial volume of 370 mm^3. The pE of the pore solution was 2.54, which is typical of cement where sulphides are not present (Glasser, 1992).

The composition of the mineral assemblage was formulated through an optimisation procedure (using a non-linear generalized reduced gradient algorithm) to modify the proportions of a group of probable cement hydration products until the chemical composition of the assemblage matched the oxide analysis of the cements. CSH gel was included in this group and its Ca/Si ratio allowed to vary within probable limits (0.7 – 2.3). The compositions provided in Table 11 are the ones arrived at by this process. This process was chosen rather than using the mineralogical composition determined using powder X-ray diffraction on the grounds that the pastes were found to be incompletely hydrated at 28 days, but were likely to undergo further hydration during acid exposure. The solubility products and stability constants of cement hydration products and dissolved species were those used by Lothenbach, Matschei, Möschner and Glasser (2008). More general speciation and solubility data were from the Minteq database (U.S. Environmental Protection Agency, 1999). The decalcification of CSH gel was dealt with by including three forms of CSH gel with Ca/Si ratios of 0.8, 1.1 and 1.8, plus silica gel, an approach previously adopted by De Windt and Devillers (2010). The solubility products used by these researchers were employed.

Diffusion between the tank and the interior cells of the cement paste was modelled using PHREEQC's TRANSPORT keyword. Boundary conditions were set such that either end of the configuration were closed. PHREEQC employs a single diffusion coefficient for all dissolved species, which is unlikely to be the case in reality. Furthermore, it does not readily permit changes in diffusion coefficients resulting from changes in microstructure. However, geochemical modelling was used in this study as a means of further examining the deterioration mechanisms, and so these limitations were considered acceptable. A value for the diffusion coefficient was obtained by adjusting it until an adequate fit (within 0.5 of a pH unit) between the measured and modelled pH in the exposure solution at the end of the exposure period was obtained.

RESULTS

Mass loss

Figure 2 shows the manner in which the mass of cement paste specimens exposed to the lactic acid solution changed with time, along with the pH of the exposure solution. Mass loss from all specimens is evident, with the most rapid loss displayed by the CSA paste and the least by the PC paste.

In the case of citric acid (Figure 3), the rate of mass-loss was so rapid that measurements were stopped after an exposure period of 14 days. As has been observed by other researchers, copious quantities of white precipitate was observed to form around the specimens. The lowest rate of mass-loss was displayed by the CSA specimen, whilst the PC/FA specimen lost the most mass. The opposite trends were observed in the case of tartaric acid (Figure 4), with substantial mass-loss from the CSA specimen. The PC and PC/FA specimens developed a crust of reaction products at their surface. It was noted that removal of these specimens from the solution using tongs would sometimes break off a quantity of this crust. Thus, the act of measurement was partly responsible for the observed mass-loss.

Figure 5 shows mass loss from the specimens exposed to catechol solutions. The solutions gradually turned black with time and the specimens also took on a black colour. Mass loss from these specimens was notable, with the most lost from the PC/FA specimen and the least from the CSA specimen.

µCT scans

Cross-sections of the paste cylinders obtained from µCT scanning are shown in Figures 6, 7 and 8 for the PC, PC/FA and CSA specimens respectively. Examination of Portland cement pastes after acid attack by other researchers has identified the appearance of three zones (Bertron and Duchesne, 2013). These zones are an outer zone in which decalcification of the paste is essentially complete (subsequently described as 'decalcified'), a zone beyond this where the process of decalcification is ongoing (the 'outer core'), and an inner zone which is currently unaffected by acid attack (the 'inner core'). All three zones are evident in most of the PC specimens, but not in the PC/FA and CSA specimens, where only the decalcified and inner core zones are evident. The exceptions to this are the specimens exposed to citric acid, where the majority of each specimen comprises only an inner core with a thin outer layer of decalcified material, regardless of cement type.

Substantial cracking of the decalcified zone was often observed, and in some cases this layer partially fell away from some samples during handling. Cracking was not evident immediately after specimens were removed, and it is likely it resulted from shrinkage of this layer during drying.

In the case of the PC and PC/FA specimens exposed to tartaric acid, a crust of precipitate was also present, with only a thin decalcified zone – most evident in the case of the PC/FA specimen. The crust appears to be exfoliating from the specimens as a series of layers. As previously discussed, this crust is described as being protective, and it should be noted that deterioration of the CSA paste, where no crust is formed, has occurred to a greater extent.

The interpretation of these images is dependent on how decalcification should be viewed with regards to cement and concrete properties. A fully decalcified layer is certainly of low strength, but it should be stressed that the partial decalcification process produces the largest drop in strength (Chang, Song, Munn and Marosszeky, 2005). This is because partial decalcification involves the removal of relatively large portlandite crystals leading to the formation of macroporosity. The lack of partial decalcification in the PC/FA and CSA pastes results from portlandite being either present in low concentrations or absent. Further decalcification leads to the formation of microporosity, which has a lesser effect on strength. For this reason, the approach taken in this paper is to use only the volume of unaffected cement paste remaining after exposure as a measure of resistance to attack.

Maintaining strength is not the only reason for requiring acid-resistance in concrete. It may also be required to maintain adequate cover, or to preserve a functional surface such as a floor or pipe interior. However, it is unlikely that the presence of a decalcified layer will satisfy either of these objectives, and the approach adopted for judging performance remains valid.

Figure 9 summarises the extent to which the different zones resulting from acid attack were present at the end of the exposure period. This is expressed in terms of the cross-sectional area occupied by the zones, which, discounting the ends of the cylinders, is directly proportional to the volume of each zone. Taking the area occupied by the inner core as a measure of acid resistance, performance of a given cement type is evidently dependent on the acid type. In the case of lactic acid, the CSA and PC/FA specimens provide the greatest resistance. This is in accordance with the general observation that where acidolysis is the main deterioration mechanism, a lower calcium content yields greater acid-resistance. For citric acid and catechol exposure (where precipitation of expansive products is

evidently the principal attack mechanism), PC and CSA perform better than PC/FA. The PC and PC/FA specimens offer greater resistance to tartaric acid, possibly as a result of the protective nature of the tartrate crust which is formed.

Two features should be noted in these results. Firstly, in many cases, the difference in acid resistance between cement types is small. Secondly, on the assumption that the persistence of the inner core zone as a measure of acid resistance is an appropriate method of interpretation, there is a lack of parity between mass-loss and CT scan results. This raises the question of whether mass loss measurements alone are an appropriate means of interpreting acid resistance.

Analysis of decalcified layers and reaction product crusts

Figure 10 shows the powder X-ray diffraction traces obtained from the acid-affected layers taken from the paste specimens. The quantities of crystalline constituents in these layers, estimated using Rietveld refinement of the XRD traces, are given in Table 12, alongside the original composition of the hydrated pastes prior to exposure to the acid solutions. Table 13 shows the chemical composition of the crusts determined by XRF.

Lactic acid

In the case of the lactic acid, only amorphous material remains in the affected layers, whilst the crystalline material present in the PC/FA and CSA pastes are residual phases from the pastes prior to exposure to acid which are highly insoluble: quartz and mullite in the paste containing FA and perovskite and gibbsite in the CSA paste.

Citric acid

In the case of PC and PC/FA pastes exposed to citric acid, phases presumed to be calcium citrate compounds were precipitated – identified as Phases A and B on the traces. Phase A has previously been identified as earlandite ($Ca_3(C_6H_5O_7).4H_2O$) (Bertron and Duchesne, 2013). However, during Rietveld refinement it became evident that the phase present was structurally different from earlandite, an observation which has previously been made when comparing earlandite with calcium citrate found in pharmaceutical products (Kaduk, 2013). Phase B was only found in the PC paste, and could not be matched with any known phase. Whilst it is possible that the phase is a form of calcium citrate, the XRD pattern resembles that of an AFm phase, albeit one with a relatively large interlayer spacing. AFm phases containing intercalated organic acid ions, such as formate, have been previously encountered (Pöllmann, Kaden and Stöber, 2014), and there exists the possibility of a citrate AFm phase having been formed. For the above reasons, Rietveld refinement was not possible on the PC and PC/FA affected layers. Where the CSA paste has been exposed to citric acid, similar results to those obtained for lactic acid were observed, with the exception that gehlenite remains from the original paste.

Tartaric acid

The PC and PC/FA pastes exposed to tartaric acid form a crust of calcium tartrate tetrahydrate, which also contains a quantity of amorphous material. The CSA paste does not form a tartrate crust.

However, it does form a phase with a cubic unit cell with a similar pattern to that of hydrosodalite ($Na_6(AlSiO_4)_6.8H_2O$). However, the absence of sodium in the affected layers (Table 13) means that complete substitution by other elements for sodium is likely. The most likely candidate is calcium. Partial substitution of calcium for sodium in hydrosodalite has been observed previously (33% by mass) (Kendrick and Dann, 2004), producing a shift in unit-cell length from 8.768 to 8.951 Å. The phase observed in the affected layer of the CSA paste has a unit-cell length of 9.078 Å, which would be in agreement with a higher level of calcium substitution. On the assumption that the phase present possessed the chemical formula $Ca_3(AlSiO_4)_6.8H_2O$, a structure representing hydrosodalite with 100% Ca substitution was used in the Rietveld refinement process. The formation of a hydrosodalite phase is presumably the result of complexation of Al^{3+} (Table 6), with higher dissolved concentrations permitting formation of the compound.

Catechol

The PC paste exposed to a catechol solution contains calcite and thaumasite ($Ca_3Si(OH)_6(CO_3)(SO_4).12H_2O$). In both cases it is unlikely that these phases were formed during the exposure process, since the containers used for this were air-tight and had only a small air-space above the solution, limiting the extent to which carbon dioxide could dissolve in the solution and react with the specimen. It is more likely that carbonation of portlandite and possibly other hydration products has occurred during the drying process, leaving calcite. This indicates a higher concentration of calcium in the affected layer compared to other PC specimens (Table 13). The formation of thaumasite is presumably partly the result of the presence of calcite providing a source of carbonate. However, thaumsite formation would not normally be expected in these circumstances. It would appear that the presence of catechol has acted to enable the formation of thaumasite, presumably through its ability to form complexes with Si^{4+} ions (Table 8).

Whilst the formation of thaumasite in this case has resulted from specimen handling, it does raise an interesting issue. Thaumasite formation is a concrete durability issue normally affecting concrete structural elements in contact with the ground, with factors such as sulfate and bicarbonate concentrations in soil and groundwater, and temperature playing important roles in influencing its occurrence (Clark, 2002). Given that catecholate groups are a common feature of humic acid molecules, this result points to another possibly significant factor – concentrations and chemical characteristics of humic acids, or other organic molecules capable of forming complexes with Si^{4+}, in soil.

Amorphous phase composition

Using the results of Rietveld refinement from Table 12 and the chemical analyses from Table 13, it was possible to estimate the composition of the amorphous phases in the affected layers. These are shown in terms of CaO, Al_2O_3 and SiO_2 content in the form of ternary diagrams in Figure 11. Also plotted on these diagrams are the compositions of the amorphous fraction of the hydrated cements prior to acid exposure, with arrows indicating the trajectory of the process of alteration resulting from acid exposure. In the case of the pastes exposed to lactic acid, the change is principally that of decalcification. This is indicated by a shift of the position of the composition away from the calcium corner of the plot, but also by the angle of the trajectory line, which runs almost parallel to the CaO-SiO_2 axis, showing that the ratio of SiO_2 to Al_2O_3 remains relatively unchanged. This appears to be the case for the PC and PC/FA pastes, although there is some leaching of aluminium from the CSA

specimen. It has been previously noted that C-S-H gel with a lower calcium content prior to acid attack displays a tendency to be less prone to deterioration (Bertron, Escadeillas and Duchesne, 2004). This appears to be the case here, with the CSA and PC/FA pastes having lower Ca/Si ratios in the amorphous phase compared to PC, and both displaying greater resistance to acid attack.

In the case of the pastes exposed to citric acid, the plotted points corresponding to the affected layers of the PC and PC/FA specimens are not those of the amorphous phases alone, but the combined crystalline and amorphous constituents. This means that, given that calcium citrate phases were precipitated at the surface of these specimens, the leaching of calcium of the amorphous fraction alone was greater than shown in the diagram. There is some alteration of the ratio of SiO_2 to Al_2O_3 in the case of the PC/FA specimen and the CSA specimen, although it should be noted that this may also be the result of the underestimation in the extent of decalcification in the case of the PC/FA specimen.

The acid-affected layers of the PC and PC/FA pastes exposed to tartaric acid underwent less decalcification than those of the specimens exposed to lactic acid. However, the CSA specimen displays substantial loss of calcium. In all cases, the gradient of the decalcification trajectory on the plot indicates loss of aluminium. The nature of decalcification in the paste specimens exposed to catechol solutions is similar.

Geochemical modelling results

In most cases a diffusion coefficient of 5×10^{-13} m^2/s yielded a final pH of the modelled exposure solution which was appropriately close to the experimental results. However, in the case of the CSA paste specimen exposed to lactic acid, a coefficient of 3×10^{-13} m^2/s was necessary. In the case of catechol, disparity was observed between the experimental and modelled pH values. Adjustment of the diffusion coefficient in these cases provided overall model results which did not fit well with the observed results, and it was concluded that the reason for the disparity was more fundamental than simply one of mass transport rates. This aspect is discussed in greater detail later in this section, but for the purposes of modelling it was decided to employ a diffusion coefficient of 5×10^{-13} m^2/s.

For conciseness, results of modelling are presented in this paper for selected specimens and exposure conditions. Furthermore, to capture the key features of the model results, only solid phases with concentrations greater than 1×10^{-4} moles per model cell in at least one cell are presented.

Lactic acid

Figure 12 is a plot showing the concentrations of solid phases, dissolved species (total Ca, Si, Al and Fe) and pH with depth after a 90 day period of exposure to lactic acid. At the surface of the modelled cement specimen is a silica gel layer, where pH is low. This silica gel has been completely dissolved from the outside of the specimen, as a result of the low pH of this region, leading to proton-promoted dissolution of the gel. At further depths into the paste, there is a region where the pore solution pH rises significantly and CSH gel phases with lower Ca content are present. At even greater depth into the specimen is a region where high Ca CSH gel and portlandite co-exist. These features mirror the experimental results relatively closely. Similar results were also observed for the PC/FA model. Figure 13 shows the modelling results obtained for the CSA paste. Again, there is a strong resemblance between these results and the experimental data: in the model the outer layer of the specimen is entirely decalcified, consisting entirely of gibbsite and silica gel. Moving to greater depths into the

specimen sees an abrupt increase in pH, and a rapid transition to a composition reflecting unaltered cement.

Citric acid

Figure 14 shows model results obtained for a PC paste exposed to citric acid for 14 days. Whilst there are the same layers of increasing decalcification approaching the surface as seen for lactic acid, there is also a region in which calcium citrate tetrahydrate has been precipitated, coinciding with an abrupt change in pH. A pronounced decalcified zone is not observed experimentally, due to fragmentation (as discussed previously). By comparing the experimental and modelled results it seems reasonable to assume that all material outside the band of calcium citrate has broken away. Similar results were also observed for the PC/FA model. The results for the CSA model are shown in Figure 15. Calcium citrate was again formed. Although X-ray diffraction did not identify calcium citrate in the acid-affected layer of the CSA cement paste specimen, quantities of precipitate were observed to form in the solution. Thus, the loss of mass from the CSA specimen was also the result of calcium citrate formation, with the precipitated crystals entirely breaking away.

Tartaric acid

Figure 16 shows the results of geochemical modelling of a PC/FA paste in contact with a solution of tartaric acid – similar results were also obtained for the PC paste. The plot shows decalcification at the surface and the precipitation of calcium tartrate tetrahydrate. It closely resembles the μ-CT scan results, in that there is a thick crust of tartrate and silica gel located in the outer layers of the specimen and a decalcified layer located below. Examining the model results suggests that the reason for the higher calcium content of the amorphous material in the acid-affected layer of the cement paste specimen is the persistence of CSH gel. This is due to a steady shift in pH over this region, which leads to gradual decalcification of the CSH gel. The results from modelling of the CSA paste in contact with tartaric acid are shown in Figure 17. The results obtained deviate significantly from the experimental results in that the model predicts the precipitation of calcium tartrate. The reason for this difference between model and experiment is presumably that calcium was precipitated as the hydrosodalite-like phase in preference to calcium tartrate. Exploration of this possibility was not possible through modelling, since the precise nature of the phase, including its solubility, was not known.

Catechol

Figure 18 shows the results of modelling the interaction of the PC paste with a catechol solution. In the case of the catechol experiments, the pH of the modelled solution at the end of exposure did not match well with the pH of the actual solutions, regardless of the diffusion coefficient. By the end of the 90 day experimental period, the solutions in which the paste specimens were immersed displayed pH values of 9.30, 8.29 and 7.87 for PC, PC/FA and CSA respectively. In contrast, the corresponding modelled solutions had pH values of 9.56, 9.30 and 10.28.

It is possible that other processes were occurring which were not adequately dealt with by the model. This could include oxidation of catechol. However, it is notable that the discrepancy is larger for pastes with higher aluminium content. One possibility, therefore, is that aluminium is either forming additional complexes with catechol and hydroxide ions, or complexes of catechol, aluminium and

hydroxide ions are being polymerised and precipitated (Drever and Vance, 1994). A similar process (albeit without hydroxide ions) has been observed under acidic conditions (Liu and Huang, 2000).

The plot indicates precipitation of calcium hydrogen catecholate hydroxide hydrate. The absence of this salt in the XRD analysis, plus the significant loss of mass indicates that the likely mode of deterioration is through salt precipitation. This is also likely on the basis of the salt's molar volume, which is considerable. It also explains the relatively high calcium content of the amorphous constituents of the acid affected layer, since the parts with a lower calcium content have broken away.

The precipitation of calcium catecholate in the model does not appear to completely mirror the experimental observations. Whilst decalcification is evident in both the experimental and model results, the decalcified region in the model occurs alongside calcium catecholate. It is likely that this is the result of fragmentation exposing parts of the specimen in which calcium catecholate has been precipitated to the large volume of water in which the specimen is submerged. This solution will be under-saturated with regards to the precipitate, leading to its dissolution.

The behaviour of the PC/FA model (not shown) was similar to that of the PC model, with the exception that precipitation of calcium catecholate occurred at a greater depth. This was the result of the lower pH of the pore solutions in the PC/FA model causing the transition from low to high pH to occur further into the specimen. This may explain the poor performance of this material in the experimental programme, since it would lead to fragmentation of a greater quantity of material at the surface.

The model results for the CSA paste bear a closer resemblance to the experimental results, with an outer layer depleted with regards to certain elements relative to the interior of the specimen (Figure 19). However, it is clear by comparing Tables 12 and 13 that calcium is depleted in the experiment, whilst *aluminium* is depleted in the model. X-ray diffraction identified gibbsite in the altered zone of the paste, which is absent in the model. Gibbsite is least soluble at a pH of around 6 or 7, and substantially more soluble at pH of around 10, as is found at the surface of the modelled pastes. Thus, this lack of parity between the experimental and modelled pH values is almost certainly the reason for the failure of the model in this regard.

Complexolysis

Also shown in all of the plots are profiles of total concentrations of dissolved species in the modelled pore solutions. In a number of instances, evidence of complexolysis can be seen. Comparing the aluminium concentration profiles for PC specimens exposed to lactic acid and citric acid, there is a peak in Al concentration in the case of citric acid exposure. Examination of the model output shows that this is principally the result of the formation of the $Al(Citrate)_2^{3-}$ complex, in contrast to negligible complex formation by lactic acid. In the case of tartaric acid, a heightened concentration of dissolved Al is observed in the outer region of the modelled paste, again the result of complex formation ($Al(Tartrate)^{2-}$). Indeed, the poor performance of the CSA paste exposed to tartaric acid may partly be the result of complexolysis. Additional evidence of this is seen in the experimental data, with the change in composition of the amorphous phases of the cement pastes indicating removal of aluminium as well as calcium. However, accelerated deterioration is not seen in the model, presumably because changes in diffusion coefficients with acid attack are not addressed.

Complexolysis does not appear to be a major process in the case of catechol: Al complexes are only formed with the fully deprotonated catecholate ion, which is only present in significant concentrations at high pH, due to its high pK_a values (Table 1). Iron behaves in a similar manner. In the case of silicon,

only citric acid and catechol form complexes, and in both cases the compounds appear to have little influence of removal of this element from the modelled pastes. In the case of citric acid, this is the result of the weak complex that is formed, whilst the high pH required for full dissociation and complex formation is the reason for the failure of catechol to have any significant influence.

ACKNOWLEDGEMENTS

The author would like to thank Mr Andrew Forsyth and Mr Chen Lu for assistance with the experimental work reported in this paper. The author also wishes to acknowledge the use of the EPSRC-funded National Chemical Database Service hosted by the Royal Society of Chemistry.

CONCLUSIONS

Examination of the behaviour of cement pastes made from Portland cement, a combination of fly ash and Portland cement, and a calcium sulfoaluminate cement in contact with organic acid solutions has identified a number of important points:

- The ability of the different cements in resisting attack from different organic acids varies depending on the type of acid and the effective deterioration mechanism.
- Where acidolysis is the principal mechanism (i.e. in the case of lactic acid) cements with a low calcium content provide greater resistance.
- Where precipitation of salts is the main cause of deterioration (in the case of citric acid and catechol), both CSA and PC perform well. The reason for these similar results, however, would appear to be the result of different processes.
- In the case of tartaric acid attack, the formation of a protective crust would appear to be a factor, with CSA performing poorly as a result of an absence of a crust. However, complex formation with aluminium also appears to play a role in the deterioration of CSA cement paste in this case.
- It is notable that whilst different cements displayed different levels of acid resistance, the magnitude of this difference was, in most cases, slight. Thus, design of concrete mixes to resist acid attack requires approaches extending beyond just the selection of cement type, the most obvious being the reduction of water/cement ratio.
- Geochemical modelling of acid attack successfully simulated the processes occurring in real pastes in most cases. The exceptions to this were CSA paste in contact with tartaric acid, where precipitation of a phase other than that predicted was observed, and in the case of catechol, where the lack of parity between experimental and modelled results appears to be partly the result of precipitation of aluminium complexes, the nature of which require further investigation.
- The use of geochemical modelling has allowed the extent to which deterioration through complexolysis by organic acids is likely to occur to be probed. The accelerated removal of aluminium and iron from pastes exposed to citric and tartaric acids by this mechanism is probable. Accelerated removal of silicon by complexolysis is less likely, on the grounds that complexes formed are either weak or pH conditions are not conducive for complex formation.
- The results of geochemical modelling indicate that this technique has the potential to permit prediction of resistance of concrete and related materials to acid attack, and may be particularly useful in applications where mixtures of acids are present. However, as evidenced

by the results for catechol, it is reliant on a full complement of data regarding the aqueous chemistry of the acid being available.

REFERENCES

Adesanya DA and Raheem AA (2010) A study of the permeability and acid attack of corn cob ash blended cements. Construction and Building Materials **24(3)**: 403-409.

Apelblat A, Manzurola E, van Krieken J and Nanninga GL (2005) Solubilities and vapour pressures of water over saturated solutions of magnesium-L-lactate, calcium-L-lactate, zinc-L-lactate, ferrous-L-lactate and aluminum-L-lactate. Fluid Phase Equilibria **236(102)**: 162-168.

Berthelin J (1983) Microbial weathering processes. In Microbial Geochemistry (Krumbein WE (ed)). Blackwell Scientific Publications, Oxford, UK, pp. 223-262.

Bertron A and Duchesne J (2013) Attack of cementitious materials by organic acids in agricultural and agrofood effluents. In *Performance of Cement - based Materials in Aggressive Aqueous Environments*, *RILEM State - of - the - Art Report TC 211-PAE* (Alexander M, De Belie N, Bertron A (eds)). Springer, Dordrecht, Netherlands, pp. 131-173.

Bertron A, Duchesne J and Escadeillas G (2005) Attack of cement pastes exposed to organic acids in manure. Cement and Concrete Composites **27(9-10)**, 898-909.

Bertron A, Escadeillas G and Duchesne J (2004) Cement pastes alteration by liquid manure organic acids: Chemical and mineralogical characterization. Cement and Concrete Research **34(10)**: 1823-1835.

Bombi GG, Corain B, Sheikh-Osman AA and Valle GC (1990) The speciation of aluminum in aqueous solutions of aluminum carboxylates. Part I. X-ray molecular structure of $Al[OC(O)CH(OH)CH_3]_3$. Inorganica Chimica Acta **171(1)**: 79-83.

Burgstaller W and Schinner F (1993) Leaching of metals with fungi. Journal of Biotechnology **27(2)** 91-116.

Carde C and François R (1997) Effect of the leaching of calcium hydroxide from cement paste on mechanical and physical properties. Cement and Concrete Research **27(4)**: 539-550.

Cayot P, Guzun-Cojocaru T and Cayot N (2013) Iron fortification of milk and dairy products. In *Handbook of Food Fortification and Health: From Concepts to Public Health Applications* (Preedy VR, Srirajaskanthan R and Patel VB (eds)). Springer, New York, 2013, vol. 1, pp. 75-89.

Chang Z, Song X, Munn, R and Marosszeky M (2005) Using limestone aggregates and different cements for enhancing resistance of concrete to sulphuric acid attack. Cement and Concrete Research **35(8)**: 1486-1494.

Chapman DV (1996) *Water Quality Assessments: A guide to the use of biota, sediments and water in environmental monitoring*, 2nd ed. Taylor and Francis, London, UK.

Charlton SR and Parkhurst DL (2011) Modules based on the geochemical model PHREEQC for use in scripting and programming languages. Computers & Geosciences **37(10)** 1653-1663.

Clark LA (2002) *Thaumasite Expert Group Report: Review after Three Years' Experience.* Building Research Establishment, Garston, UK.

Dawson RMC (1959) *Data for Biochemical Research.* Clarendon Press, Oxford, UK.

De Belie N, De Coster V and Van Nieuwenburg D (1997) Use of fly ash or silica fume to increase the resistance of concrete to feed acids. Magazine of Concrete Research **49(181)**: 337-344.

De Belie N, Verselder HJ, De Blaere B, Van Nieuwenburg D and Verschoore R (1996) Influence of cement type on the resistance of concrete to feed acids. Cement and Concrete Research **26(11)**: 1717-1725.

De Windt L and Devillers P (2010) Modeling the degradation of Portland cement pastes by biogenic organic acids. Cement and Concrete Research **40(8)**: 1165–1174.

Drever JI and Vance GF (1994) Role of soil organic acids in mineral weathering processes. In *Organic Acids in Geological Processes* (Pittman ED and Lewan MD (eds)). Springer-Verlag, Berlin, Germany, 138-161.

Durning TA and Hicks C (1991) Using microsilica to increase concrete's resistance to aggressive chemicals. Concrete International **13(3)**: 42-48.

Dyer TD (2011) Characterisation of two chemical compounds formed between hydrated Portland cement and benzene-1,2-diol (pyrocatechol). Journal of Materials Science **46(16)**: 5332-5344.

Froment DH, Buddington B, Miller NL and Alfrey AC (1989) Effect of solubility on the gastrointestinal absorption of aluminum from various aluminum compounds in the rat. Journal of Laboratory and Clinical Medicine **114(3)**: 237-242.

Glasser FP (1992) Chemistry of cement-solidified waste forms. In *Chemistry and Microstructure of Solidified Waste Forms* (Spence RD (ed)). Lewis Publishers, Boca Raton, FL, USA.

Goss SL, Lemons KA, Kerstetter JE and Bogner RH (2007) Determination of calcium salt solubility with changes in pH and pCO_2, simulating varying gastrointestinal environments. Journal of Pharmacy and Pharmacology **59(11):** 1485–1492.

Hamada YZ, Carlson B and Dangberg J (2005) Interaction of malate and lactate with chromium(III) and iron(III) in aqueous solutions. Synthesis and Reactivity in Inorganic, Metal-Organic and Nano-Metal Chemistry **35(7)**: 515–522.

Hawthorn FC, Borys I and Ferguson RB (1982) Structure of calcium tartrate tetrahydrate. Acta Crystallographica **B38**: 2461-2463.

Haynes WM (2014) *CRC Handbook of Chemistry and Physics*, 95th edition. CRC Press, Boca Raton, FL, USA.

Herdtweck E, Kornprobst T, Sieber R, Straver L and Plank J (2011) Crystal structure, synthesis, aund properties of tri-calcium di-citrate tetra-hydrate $(Ca_3(C_6H_5O_7)_2(H_2O)_2).2H_2O$. Zeitschrift für Anorganische und Allgemeine Chemie **627**: 655-659.

Kaduk JA (2013) Crystal structures of group 2 citrate salts, abstract from ICDD Annual Spring Meetings. Powder Diffraction **28(2)**: 146.

Kendrick E and Dann S (2004) Synthesis, properties and structure of ion-exchanged hydrosodalite. Journal of Solid State Chemistry **177(4-5)**: 1513–1519.

Khedr SA and Abou-Zeid MN (1994) Characteristics of silica-fume concrete. Journal of Materials in Civil Engineering **6(3)**: 357-375.

Kim H-S, Lee S-H and Moon H-Y (2007) Strength properties and durability aspects of high strength concrete using Korean metakaolin. Construction and Building Materials **21(6)**: 1229-1237.

Kortüm G, Vogel W and Andrussow K (1961) *Dissociation Constants of Organic Acids in Aqueous Solution*. Butterworths, London, UK.

Lebedev AV, Ivanova MV, Timoshin AA and Ruuge EK (2007) Effect of group II metal cations on catecholate oxidation. ChemPhysChem, **8(12)**: 1863–1869.

Liu C and Huang PM (2000) Catalytic effects of hydroxyl-aluminum and silicic acid on catechol humification. In *Humic Substances. Versatile Components of Plants, Soil and Water* (Ghabbour EA and Davies G (eds)). Royal Society of Chemistry, Cambridge, UK, pp. 37-51.

Lothenbach B, Matschei T, Möschner G and Glasser FP (2008) Thermodynamic modelling of the effect of temperature on the hydration and porosity of Portland cement. Cement and Concrete Research **38(1)**: 1–18.

Lutterotti L (2010) Total pattern fitting for the combined size-strain-stress-texture determination in thin film diffraction. Nuclear Instruments and Methods in Physics Research B **268(3-4)**: 334-340.

Marklund E, Sjöberg S, Öhman L-O, Salvatore F, Niinistö L and Volden HV (1986) Equilibrium and structural studies of silicon(IV) and aluminium(III) in aqueous solution. 14. Speciation and equilibria in the aluminium(III)-lactic acid-OH^- System. Acta Chemica Scandinavica **A40**: 367-373.

Martell AE and Smith RM (2004) Critical Selected Stability Constants of Metal Complexes Database, Version 8.0 for Windows. National Institute of Standards and Technology, Gaithersburg, MD, USA, See http://www.nist.gov/srd/nist46.cfm (accessed 07/06/2016).

Mehta PK (1985) Studies on chemical resistance of low water/cement ratio concretes. Cement and Concrete Research **15(6)**: 969-978.

Öhman L-O, Nordin A, Sedeh IF and Sjöberg S (1991) Equilibrium and structural studies of silicon(IV) and aluminium(III) in aqueous solution. 28. Formation of soluble silicic acid-ligand complexes as studied by potentiometric and solubility measurements. Acta Chemica Scandinavica **45**: 335-341.

Öhman L-O and Sjöberg S (1983) Equilibrium and structural studies of silicon(IV) and aluminium(III) in aqueous solution – 10. A potentiometric study of aluminium(III) pyrocatecholates and aluminium(III) hydroxo pyrocatecholates in 0.6M Na(Cl). Polyhedron, **2(12)**: 1329-1335.

O'Neil MJ (2001) *The Merck Index : an encyclopedia of chemicals, drugs, and biologicals*, 13th ed. Merck, Whitehouse Station, NJ, USA.

Parkhurst DL and Appelo CAJ (2013) Description of input and examples for PHREEQC version 3--A computer program for speciation, batch- reaction, one-dimensional transport, and inverse geochemical calculations. In: *U.S. Geological Survey Techniques and Methods, Book 6, Chap. A43*. US Geological Survey, Denver, CO, USA. Available only at http://pubs.usgs.gov/tm/06/a43.

Pavlík V and Unčik S (1997) The rate of corrosion of hardened cement pastes and mortars with additive of silica fume in acids. Cement and Concrete Research **27(11)**: 1731-1745.

Pokrovski G and Schott J (1998) Experimental study of the complexation of silicon and germanium with aqueous organic species: Implications for germanium and silicon transport and Ge/Si ratio in natural waters. Geochimica et Cosmochimica Acta **62(21-22)**: 3413–3428.

Pöllmann H, Kaden R and Stöber S (2014) Crystal structures and XRD data of new calcium aluminate cement hydrates. In *Calcium Aluminates: Proceedings of the International Conference 2014* (Fentiman CH, Mangabhai RJ, Scrivener KL (eds)). IHS BRE Press, London, UK, pp. 75-85.

Scrivener KL, Cabiron J-L and Letourneux R (1999) High-performance concretes from calcium aluminate cements. Cement and Concrete Research **29(8)**: 1215–1223.

Seidell A (1919) *Solubilities of Inorganic and Organic Compounds*, 2nd ed. Van Nostrand, New York, NY, USA.

Sheldrick B (1974) Calcium hydrogen citrate trihydrate. Acta Crystallographica **B30**: 2056-2057.

Siad H, Mesbah HA, Khelafi H, Kamali-Bernard S and Mouli M (2010) Effect of mineral admixture on resistance to sulphuric and hydrochloric acid attacks in self-compacting concrete. Canadian Journal of Civil Engineering **37(3)**: 441-449.

Tamimi AK (1997) High performance concrete mix for an optimum protection in acidic conditions. Materials and Structures **30(3)**: 188-191.

Torii K and Kawamura M (1994) Effects of fly ash and silica fume on the resistance of mortar to sulfuric acid and sulfate attack. Cement and Concrete Research **24(2)**: 361-370.

U.S. Environmental Protection Agency (1999) *MINTEQA2/PRODEFA2, A geochemical assessment model for environmental systems—User manual supplement for version 4.0.* National Exposure Research Laboratory, Athens, Georgia, USA.

Zivica V and Bajza A (2001) Acidic attack of cement-based materials – a review. Part 1 – Principle of acidic attack. Construction and Building Materials **15(8)**: 331-340.

Figure 1. Configuration of the geochemical model.

Figure 2. Mass of cement paste specimens immersed in a lactic acid solution and the pH of the solution against time.

Figure 3. Mass of cement paste specimens immersed in a citric acid solution and the pH of the solution against time.

Figure 4. Mass of cement paste specimens immersed in a tartaric acid solution and the pH of the solution against time.

Figure 5. Mass of cement paste specimens immersed in a catechol solution and the pH of the solution against time.

Figure 6. µCT scan cross-sections through the PC paste cylinders after exposure to acid solutions. Straight lines indicate transitions to different zones, superimposed circle represents original cross-section.

Figure 7. µCT scan cross-sections through the PC/FA paste cylinders after exposure to acid solutions.

Figure 8. µCT scan cross-sections through the CSA paste cylinders after exposure to acid solutions.

Figure 9. Cross-sectional areas occupied by different zones from µ-CT scans of the acid-attacked cement paste cylinders.

Figure 10. Powder X-ray diffraction traces from the acid-affected layers of cement pastes exposed to acid solutions. G = Gibbsite; P = Perovskite; Q = Quartz; CT = Calcium tartrate; C = Calcite; T = Thaumasite; Ge = Gehlenite; HS? = Hydrosodalite-like phase; A & B = Calcium citrate phases.

Figure 11. CaO-SiO_2-Al_2O_3 ternary diagrams showing change in the composition of the amorphous phases of the affected layers of cement specimens exposed to acid solutions relative to their original composition. Asterisks corresponds to compositions of the whole affected layer (both crystalline and amorphous phases).

Figure 12. Profiles of solid phases and dissolved species concentrations and pH through a modelled PC paste exposed to lactic acid.

Figure 13. Profiles of solid phases and dissolved species concentrations and pH through a modelled CSA paste exposed to lactic acid.

Figure 14. Profiles of solid phases and dissolved species concentrations and pH through a modelled PC paste exposed to citric acid.

Figure 15. Profiles of solid phases and dissolved species concentrations and pH through a modelled CSA paste exposed to citric acid.

Figure 16. Profiles of solid phases and dissolved species concentrations and pH through a modelled PC/FA paste exposed to tartaric acid.

Figure 17. Profiles of solid phases and dissolved species concentrations and pH through a modelled CSA paste exposed to tartaric acid.

Figure 18. Profiles of solid phases and dissolved species concentrations and pH through a modelled PC paste exposed to catechol.

Figure 19. Profiles of solid phases and dissolved species concentrations and pH through a modelled CSA paste exposed to catechol.

Figure 1

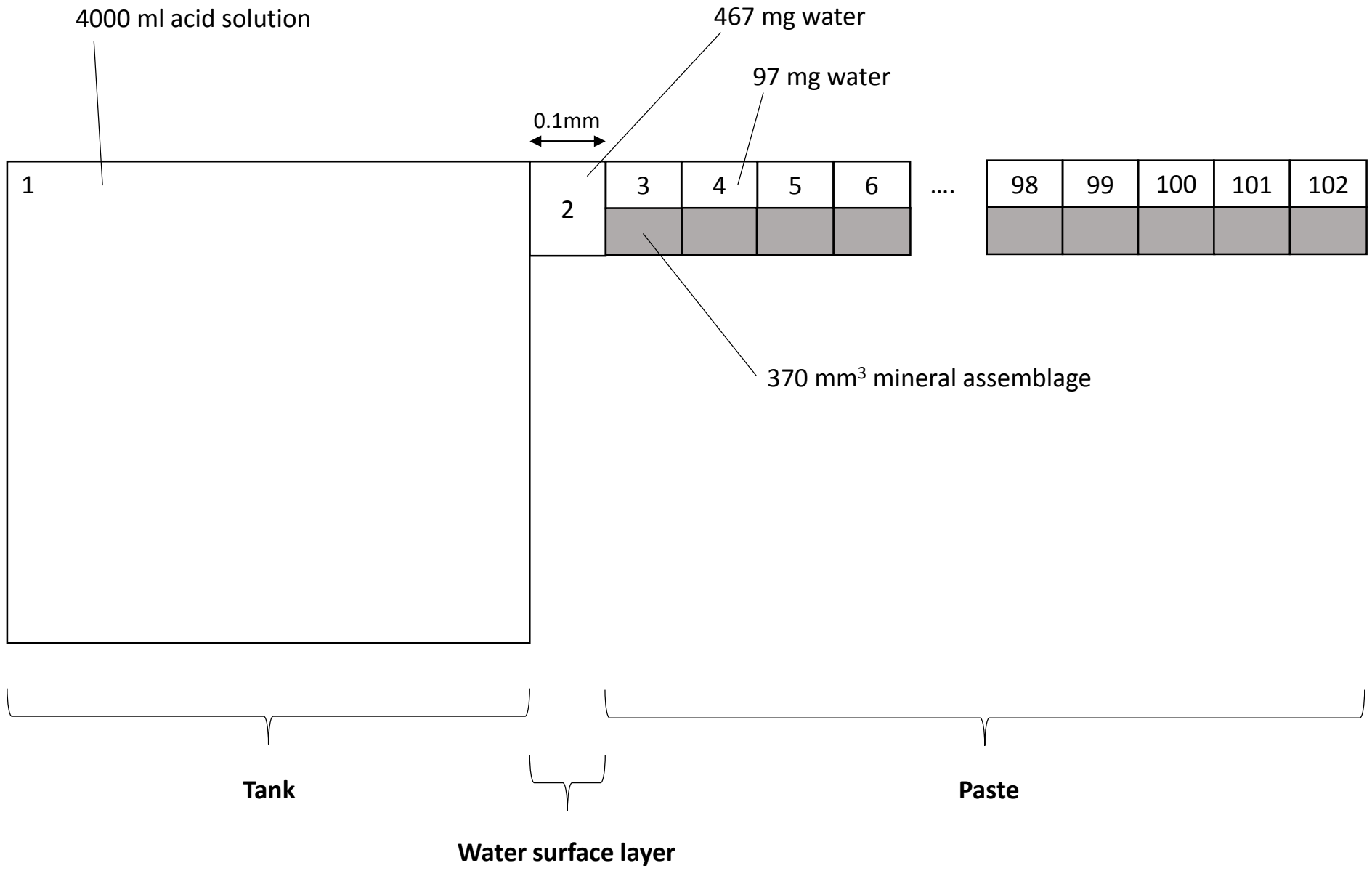
4000 ml acid solution
467 mg water
97 mg water
0.1mm
1
2
3
4
5
6
....
98
99
100
101
102
370 mm3 mineral assemblage
Tank
Water surface layer
Paste

Figure 2

Click here to download Figure Figure 2.TIF

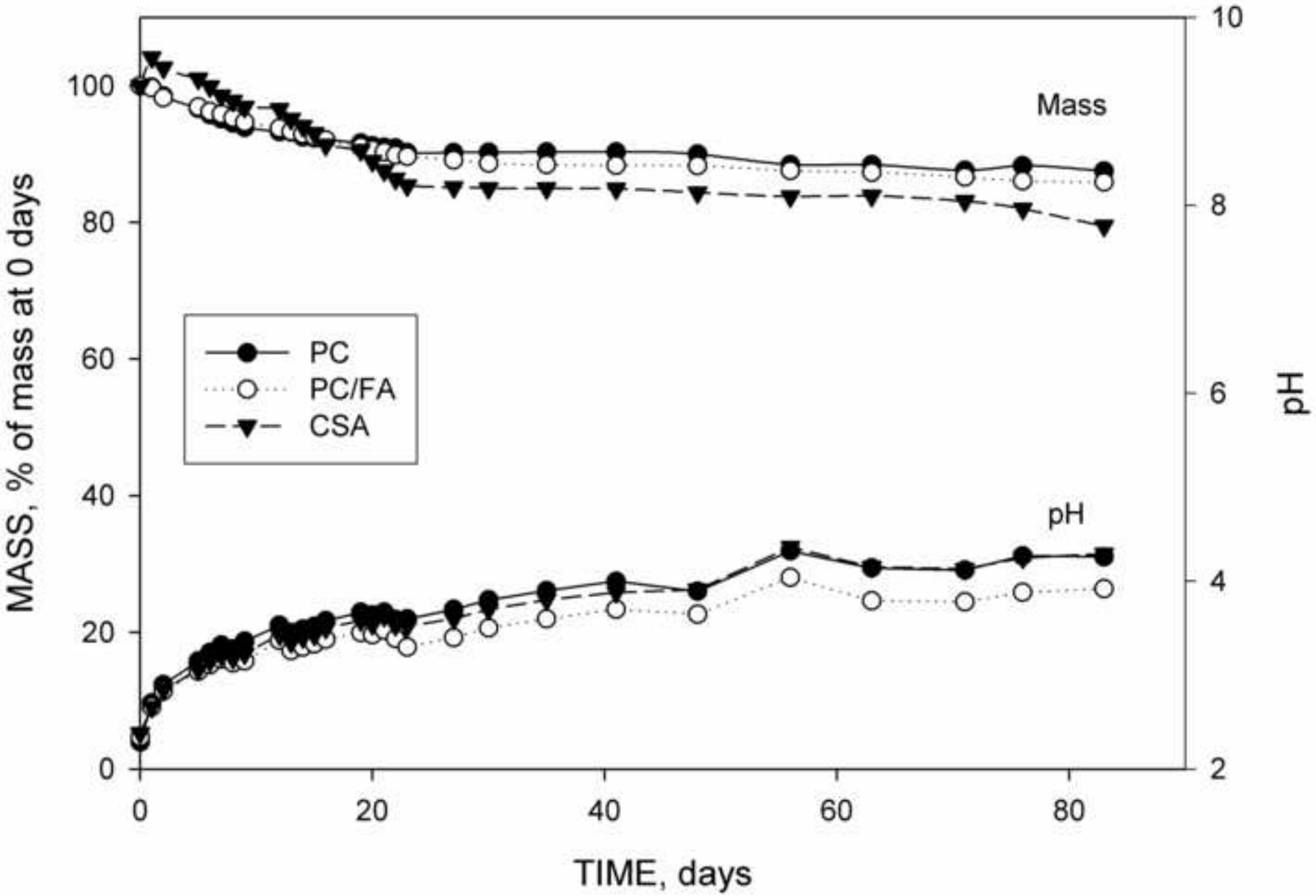

Figure 3

Click here to download Figure Figure 3.TIF

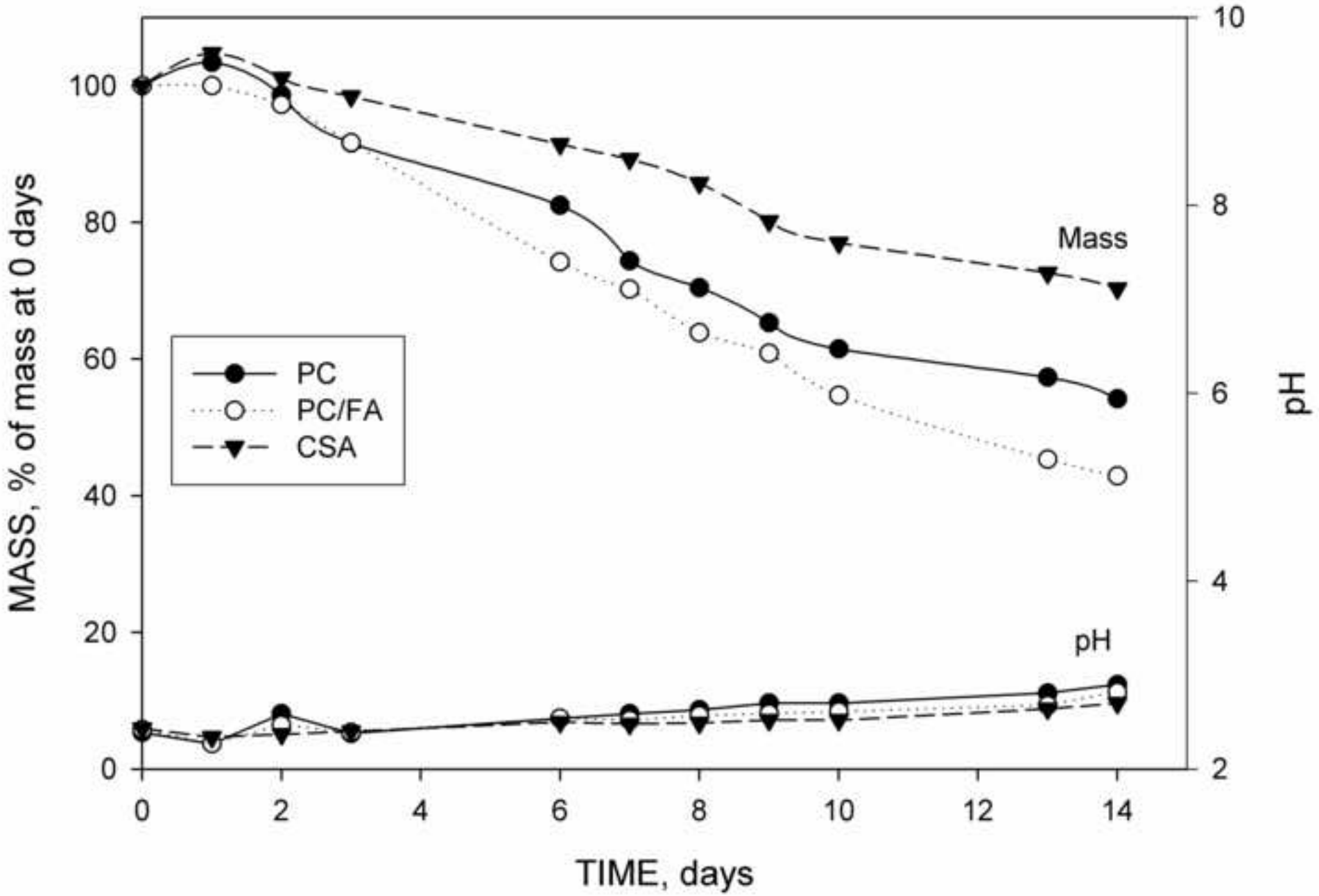

Figure 4

Click here to download Figure Figure 4.TIF

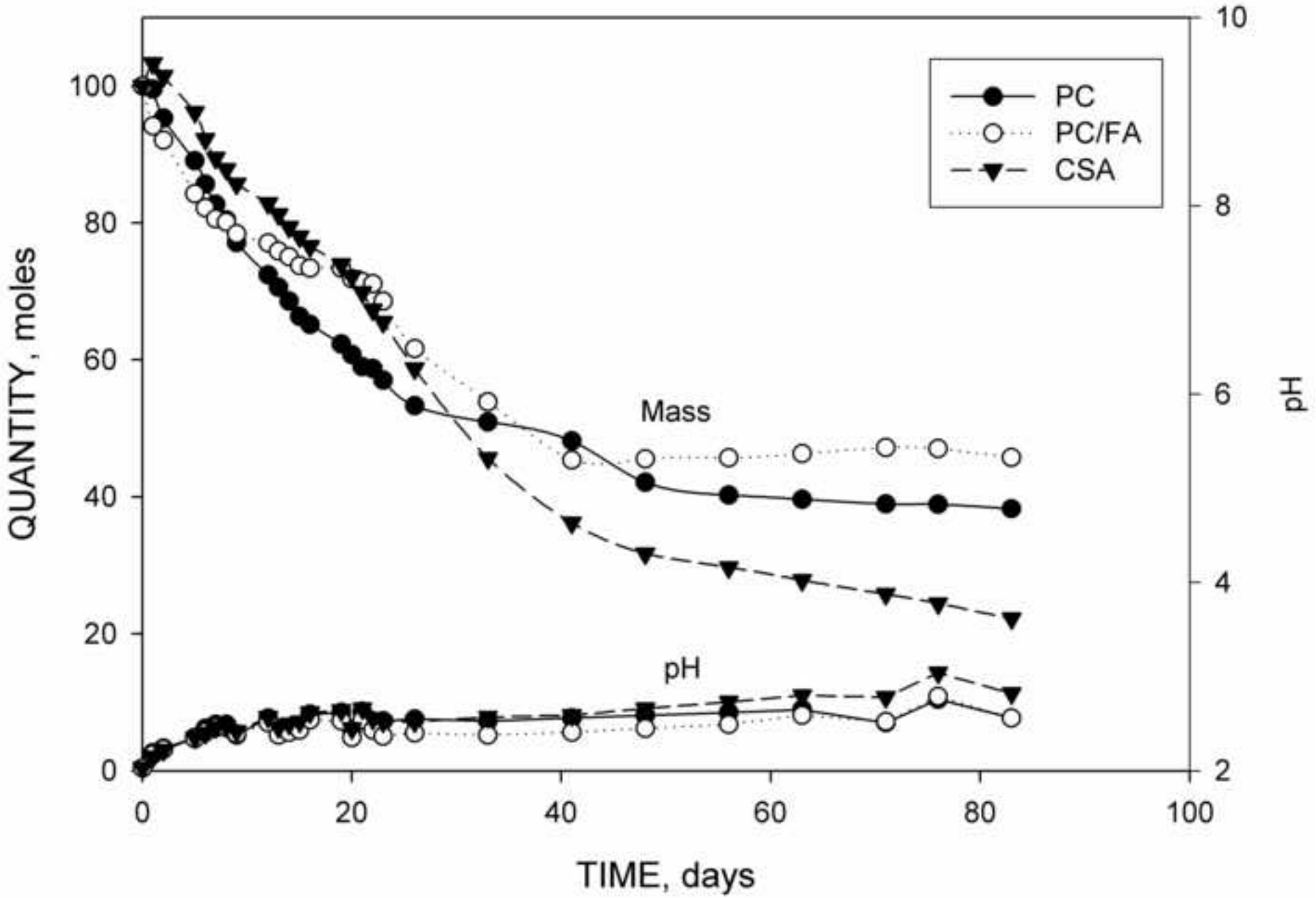

Figure 5

Click here to download Figure Figure 5.TIF

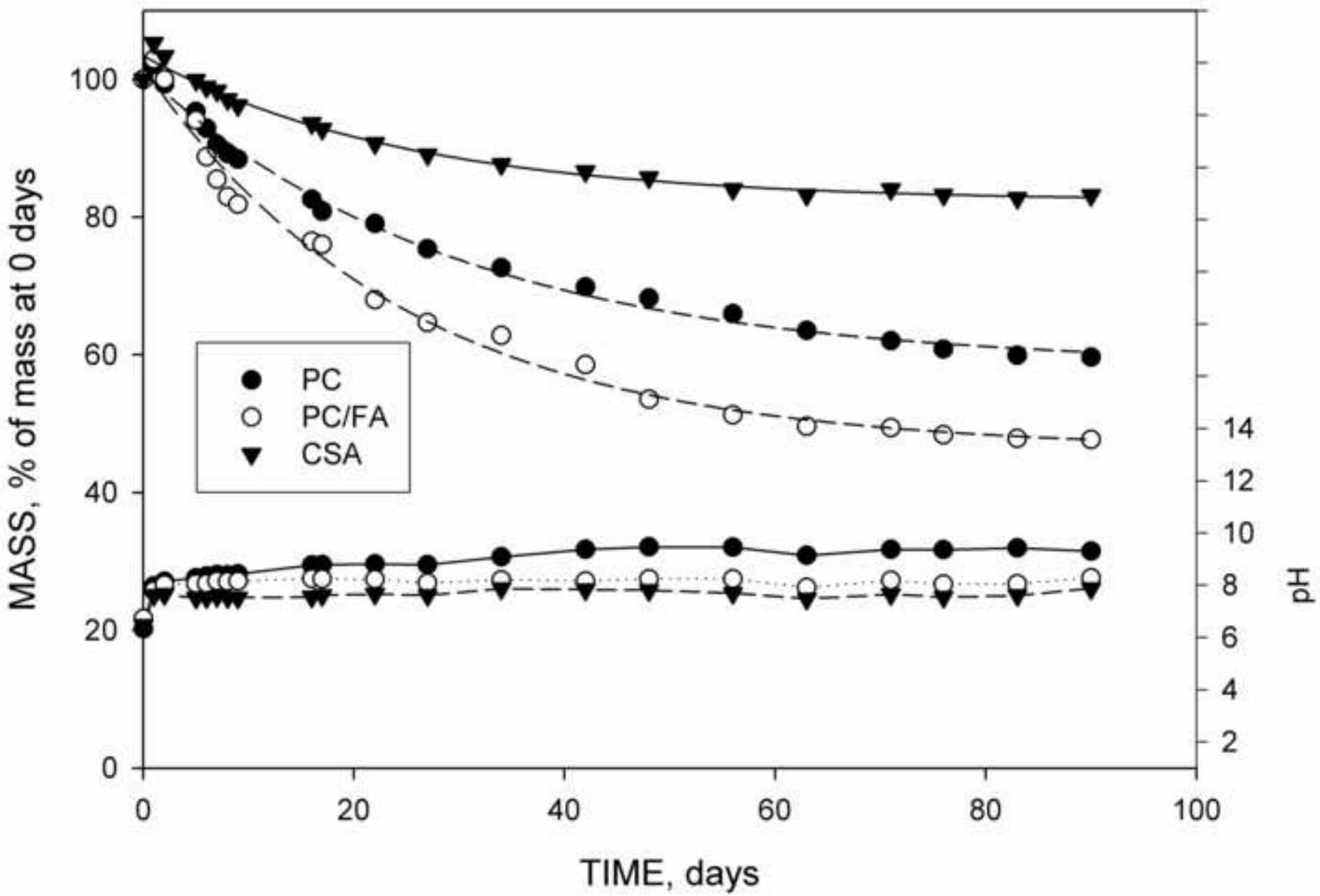

Figure 6

Click here to download Figure Figure 6 modified.tif

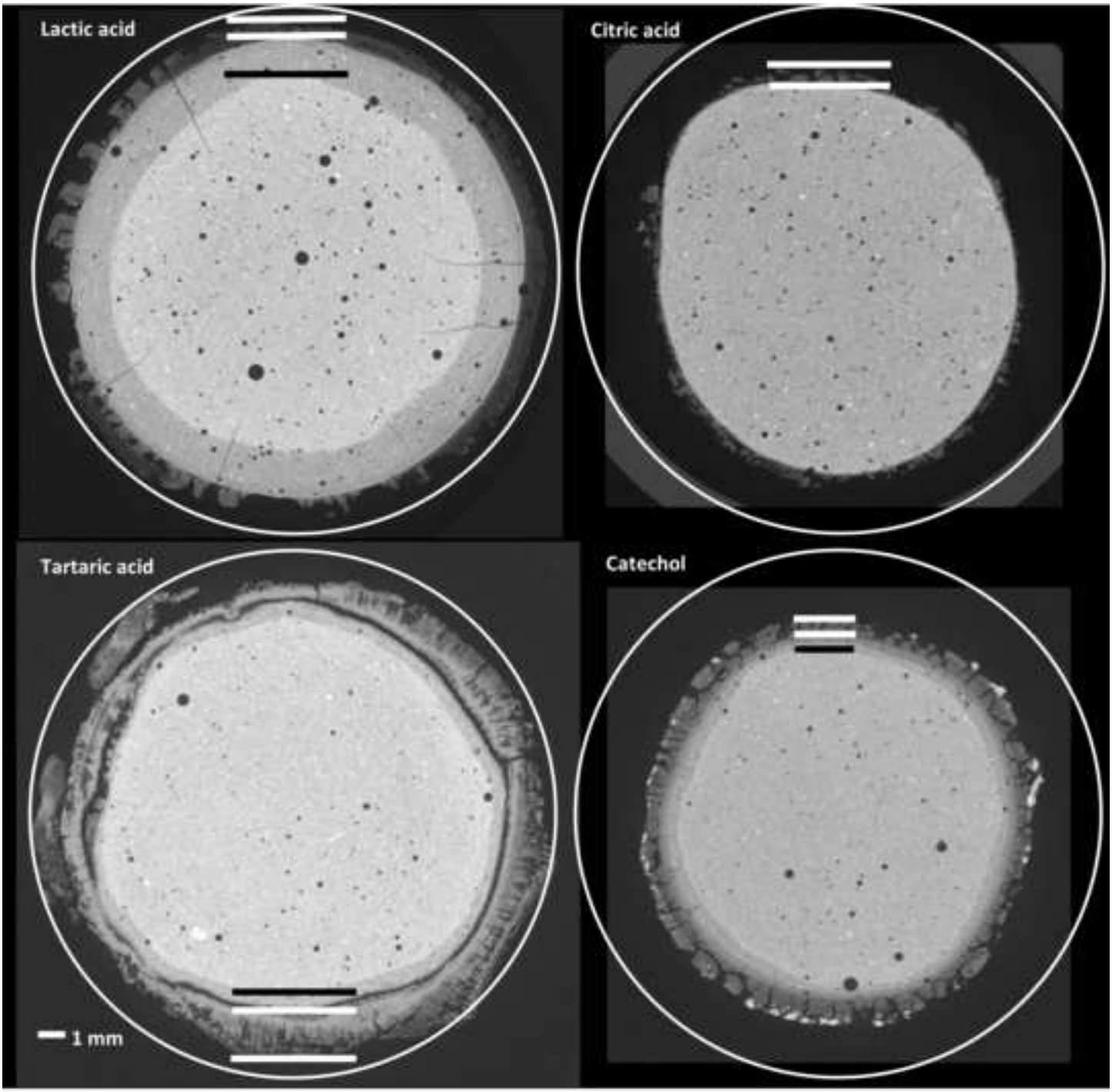

Figure 7

Click here to download Figure Figure 7 modified.tif

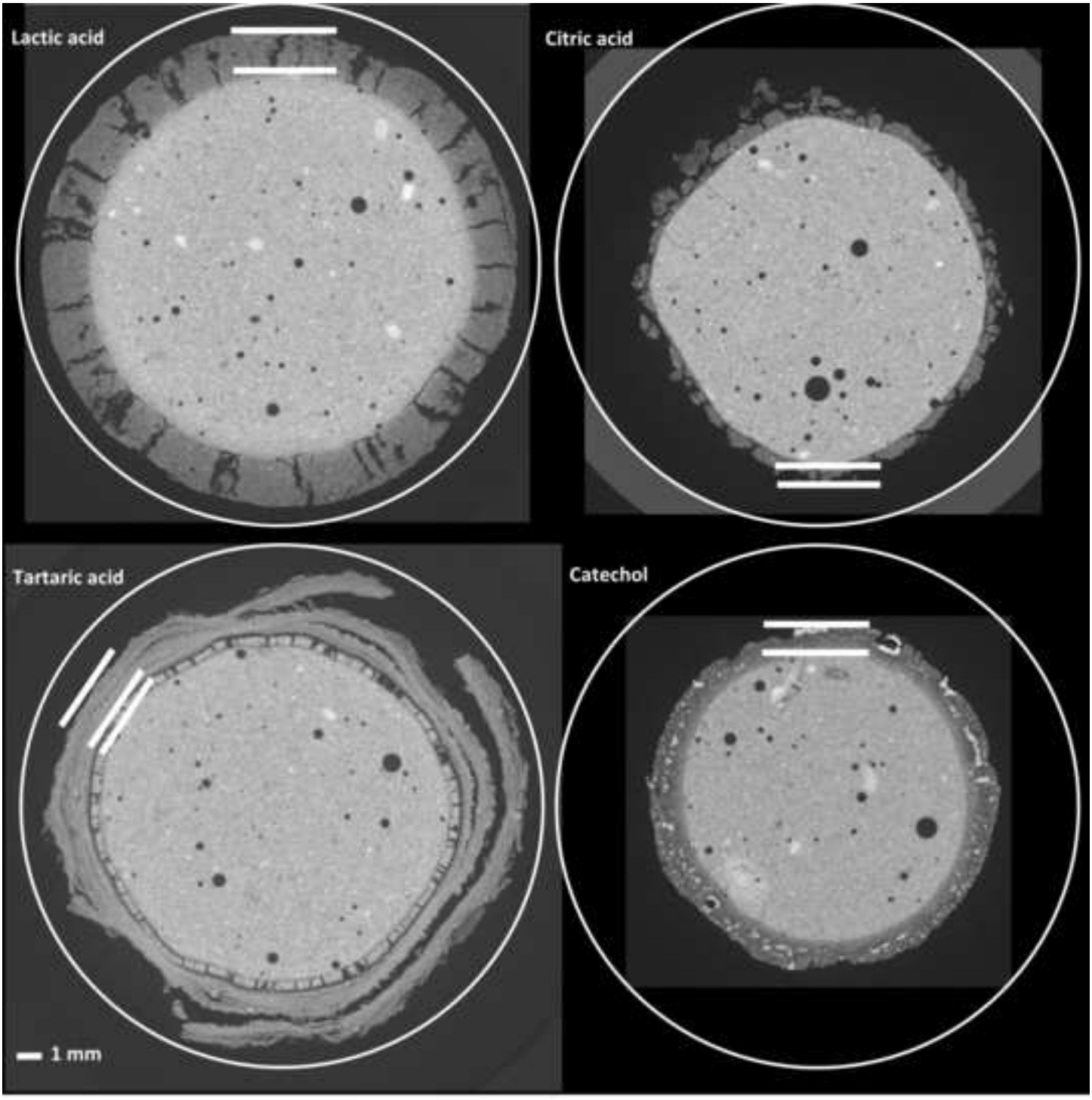

Figure 8

Click here to download Figure Figure 8 modified.tif

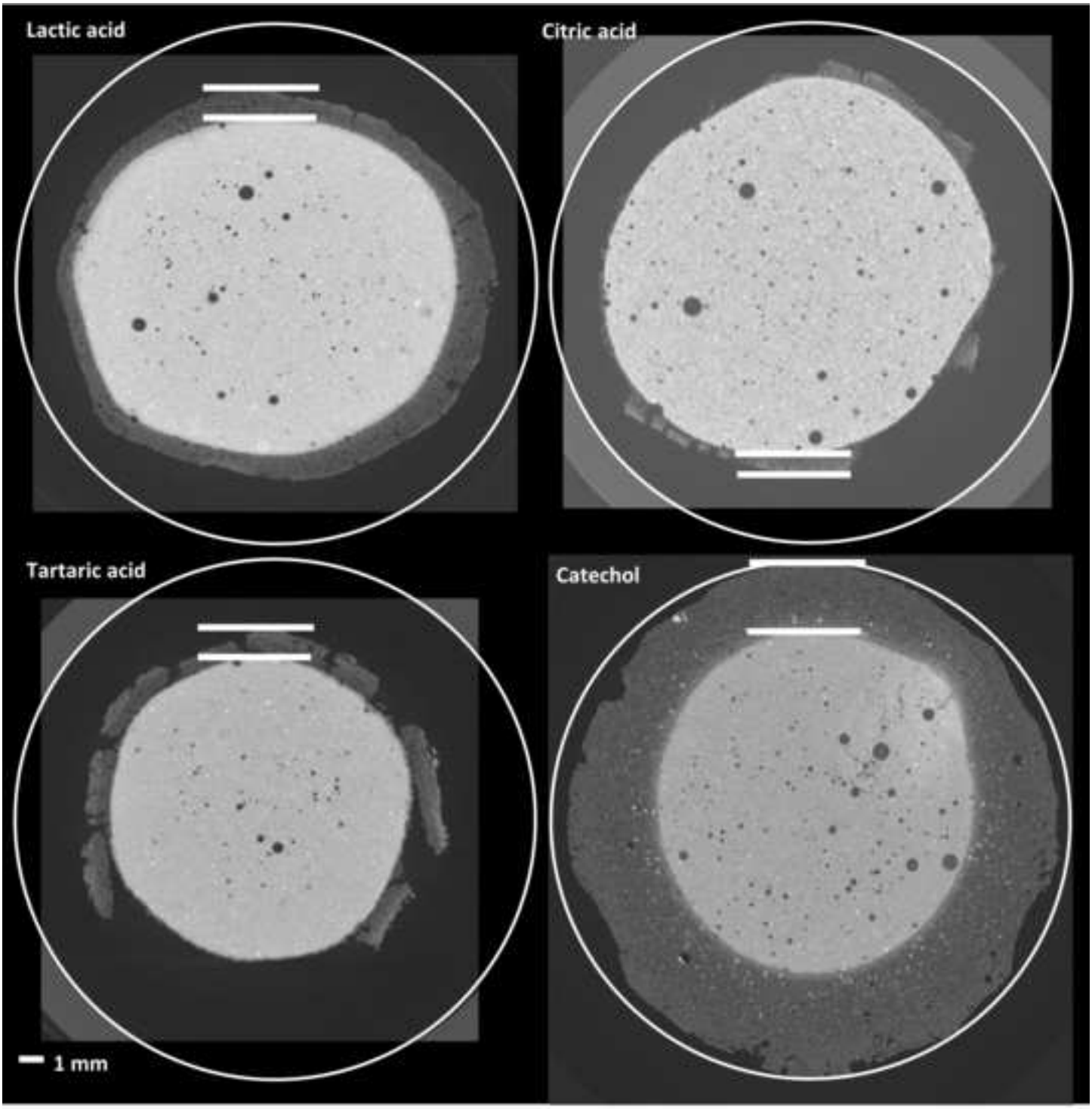

Figure 9

Click here to download Figure Figure 9.TIF

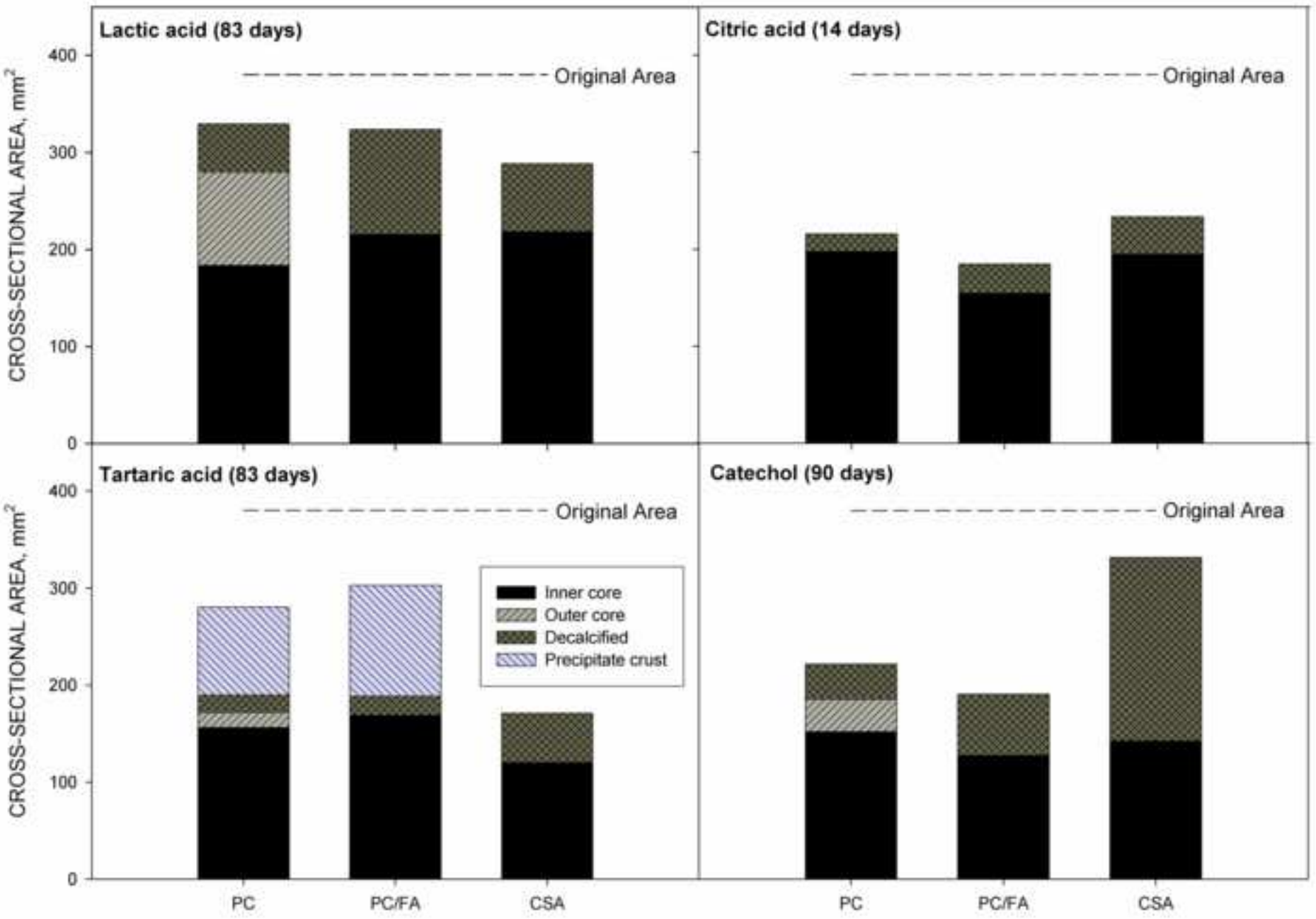

Figure 10

Click here to download Figure Figure 10.TIF

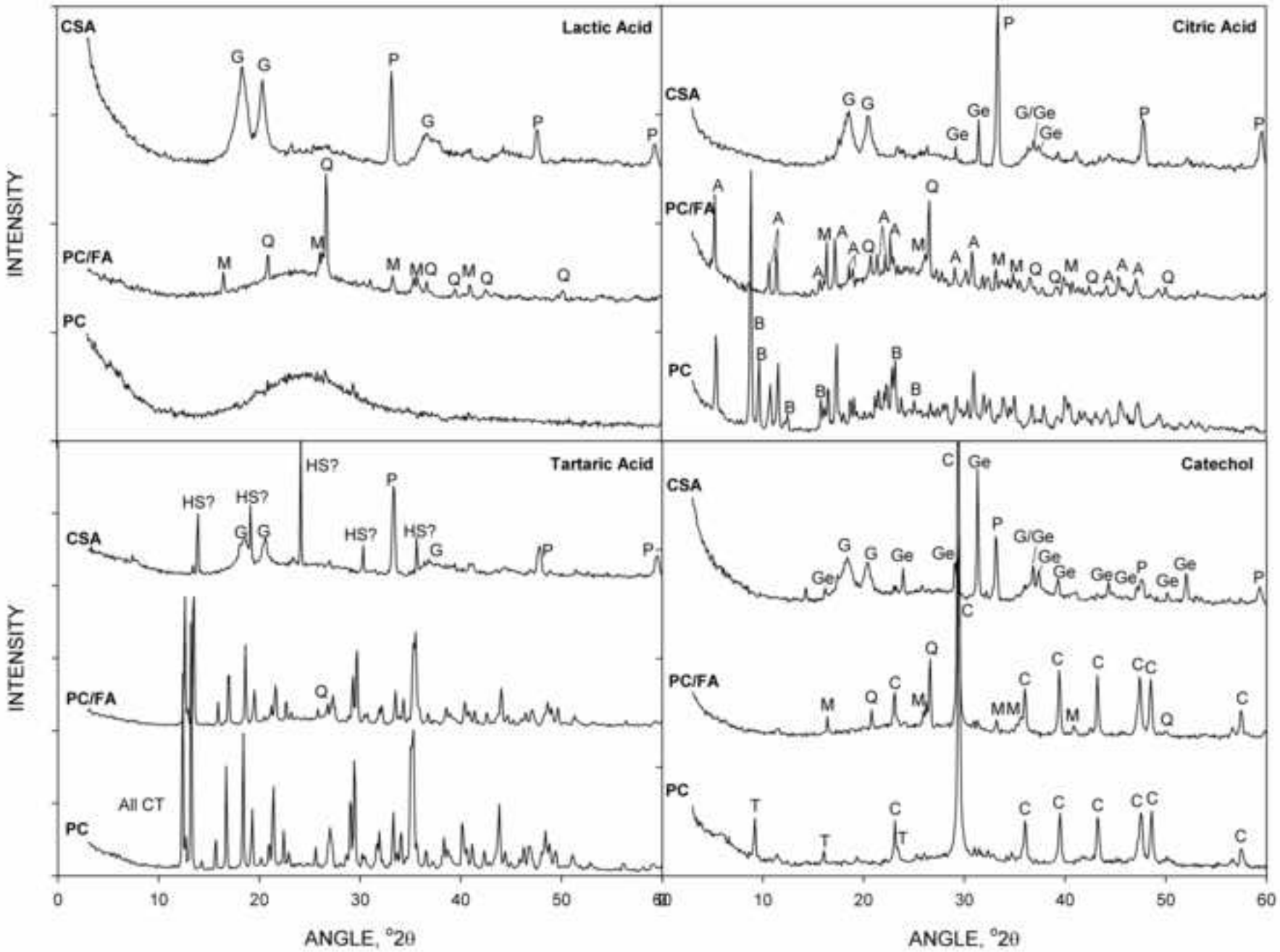

Figure 11

Click here to download Figure Figure 11.TIF

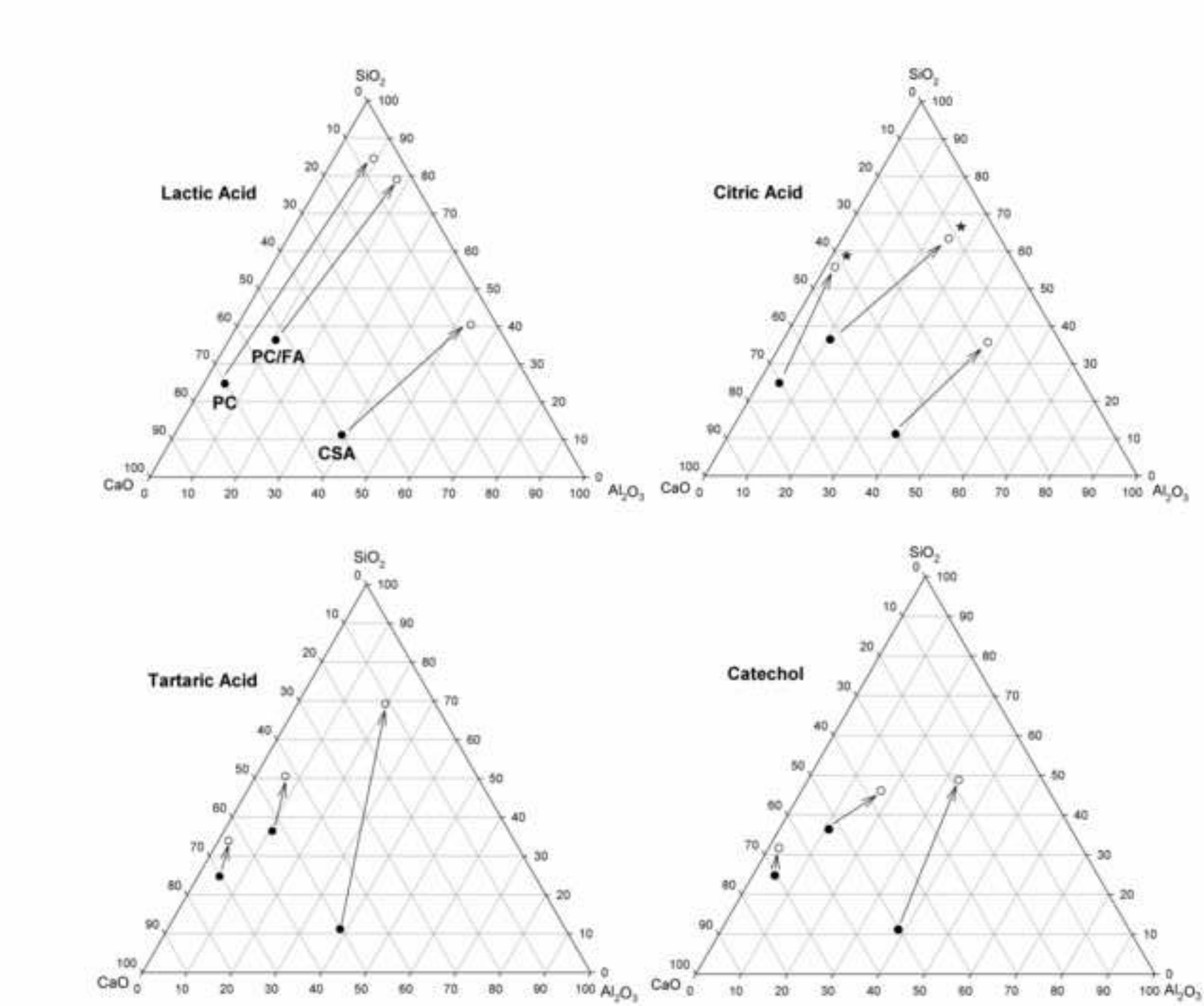

Figure 12

Click here to download Figure Figure 12.TIF

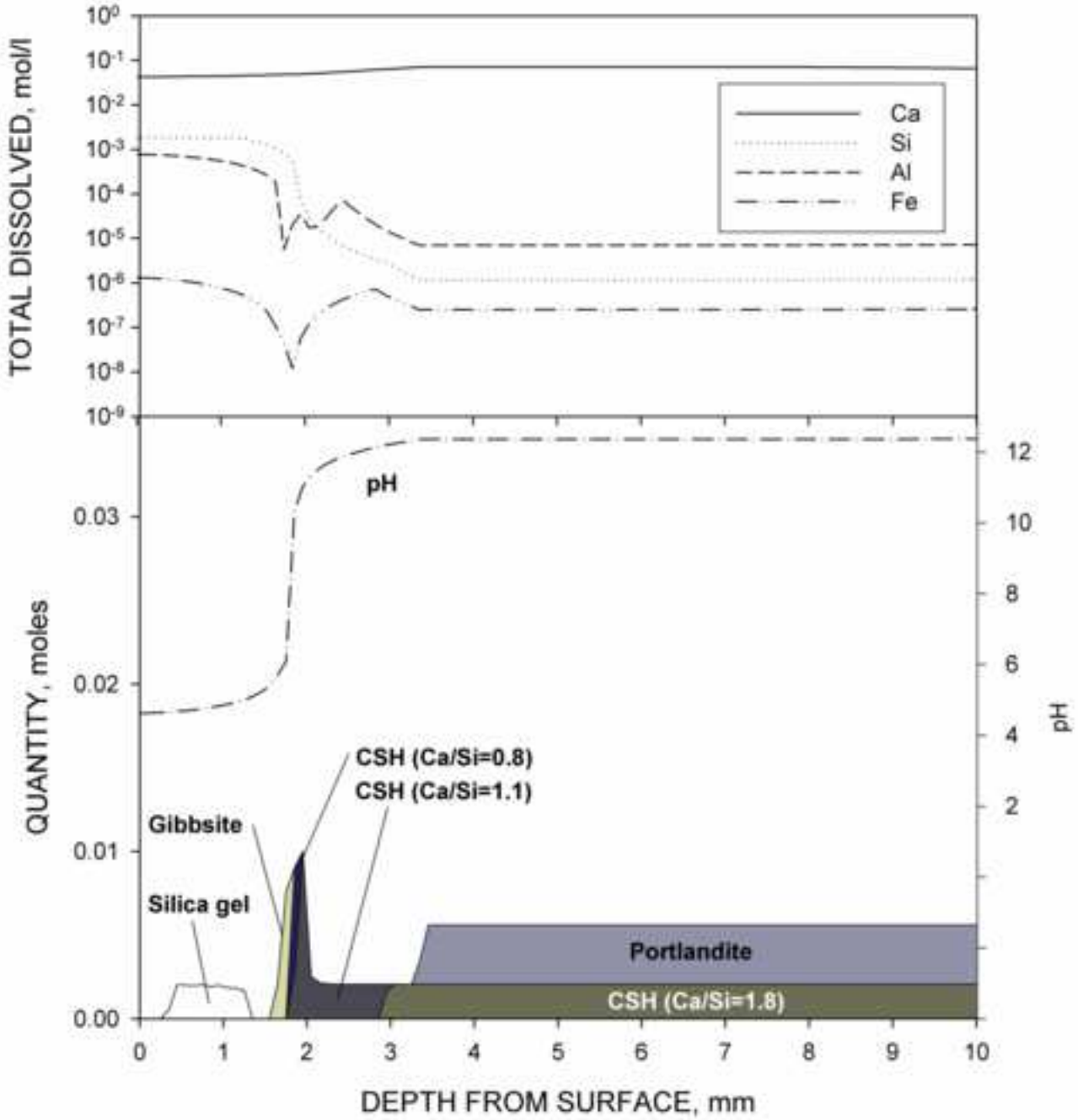

Figure 13

Click here to download Figure Figure 13.TIF

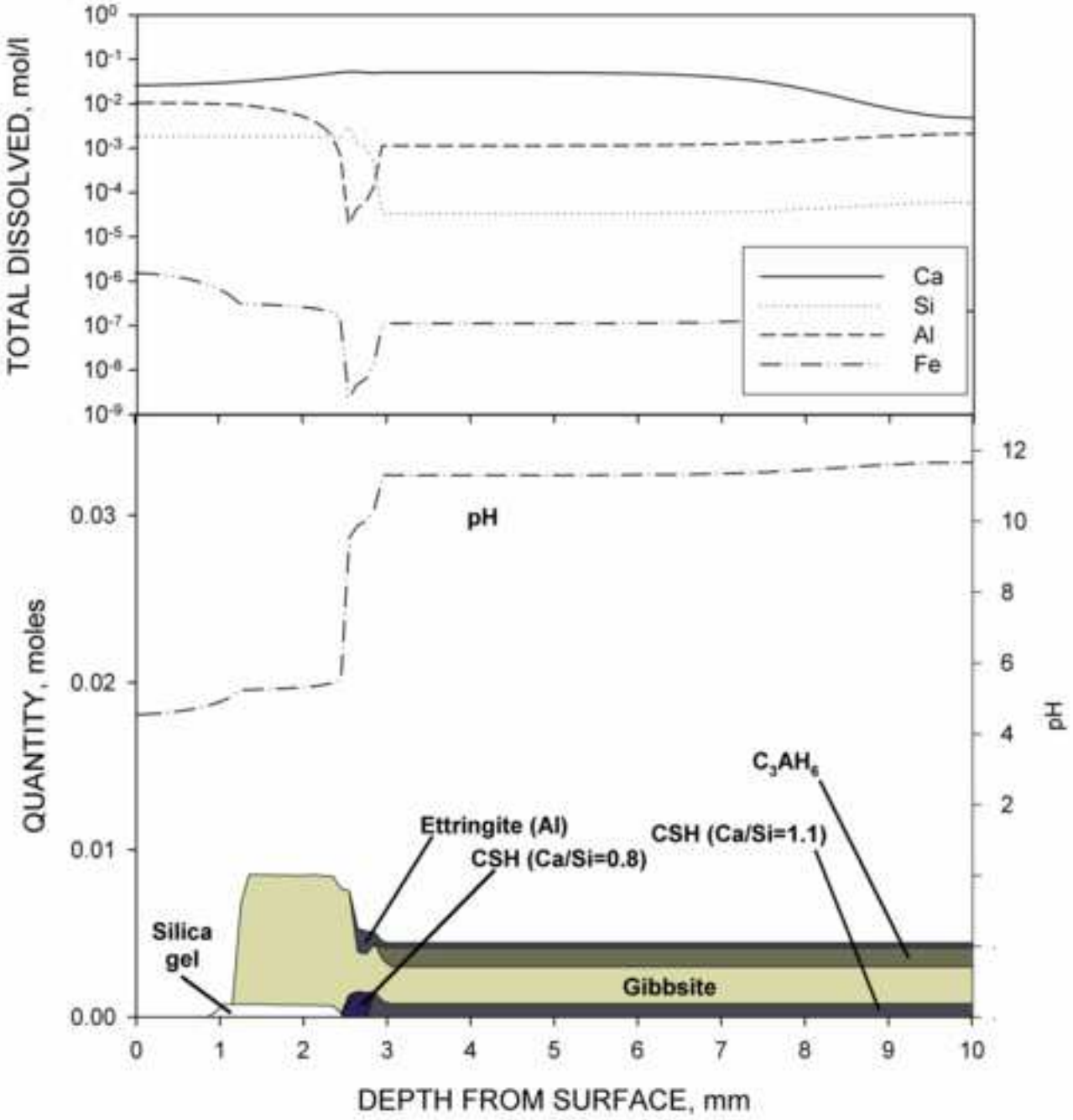

Figure 14

Click here to download Figure Figure 14.TIF

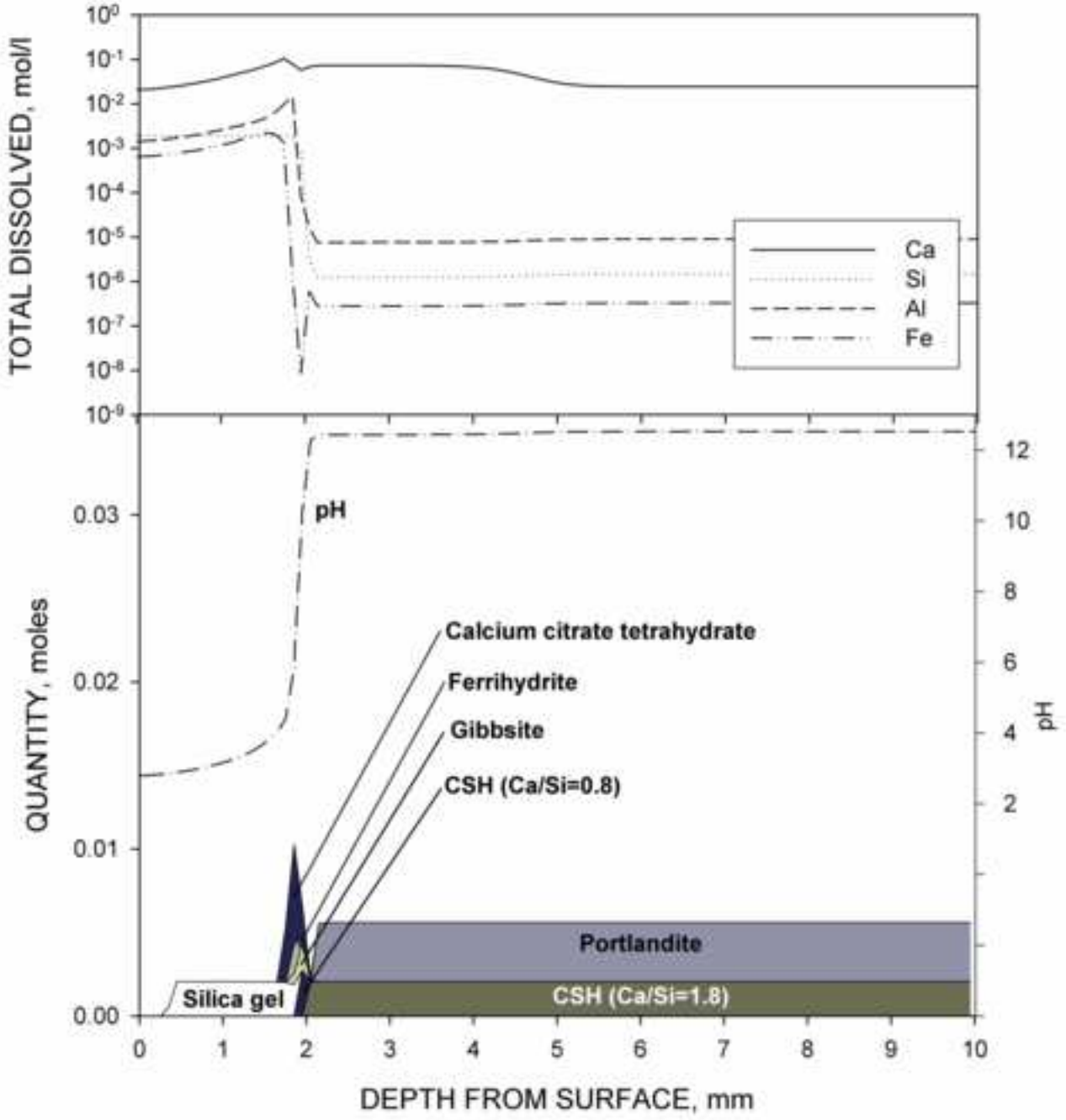

Figure 15

Click here to download Figure Figure 15.TIF

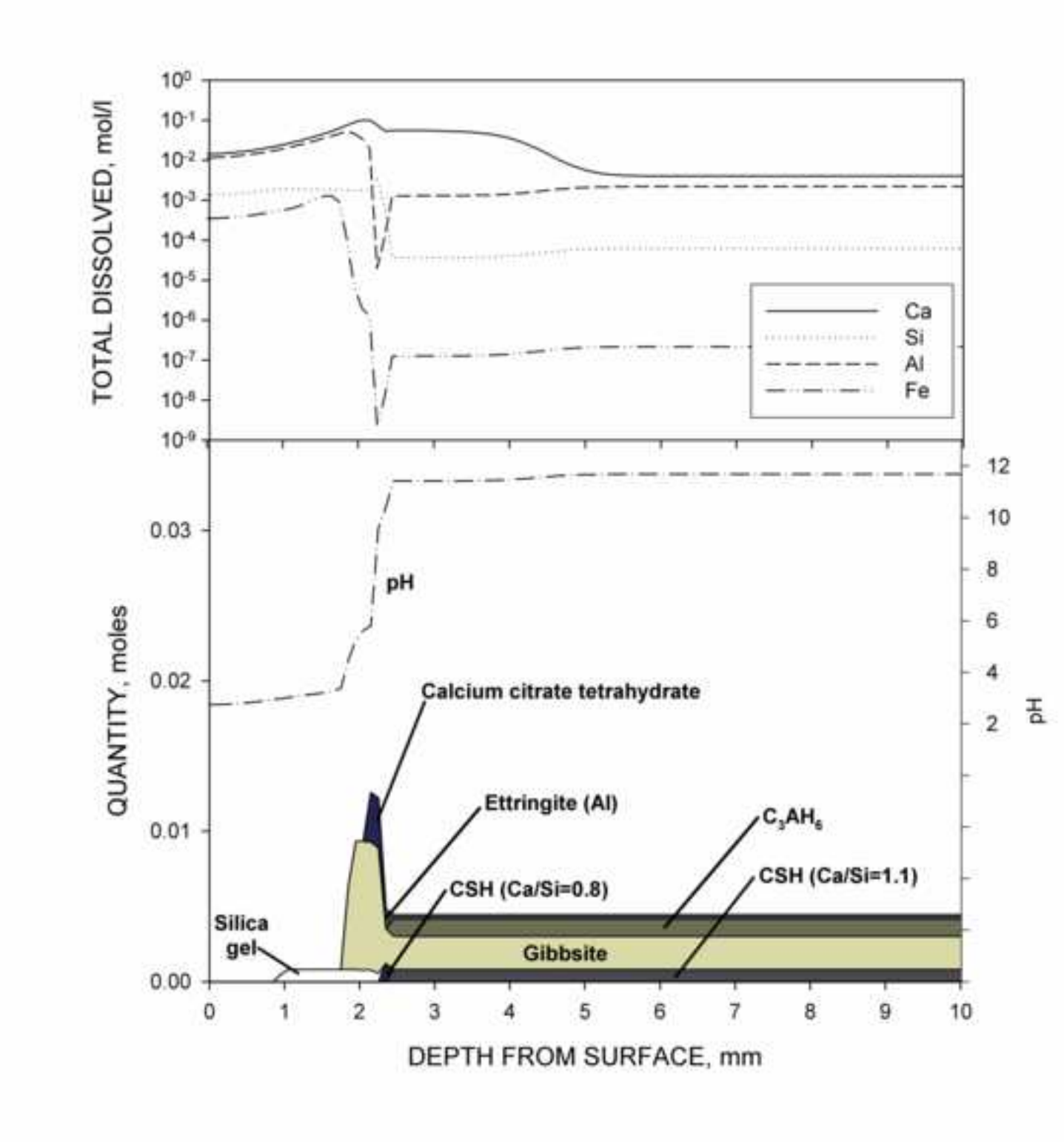

Figure 16

Click here to download Figure Figure 16.TIF

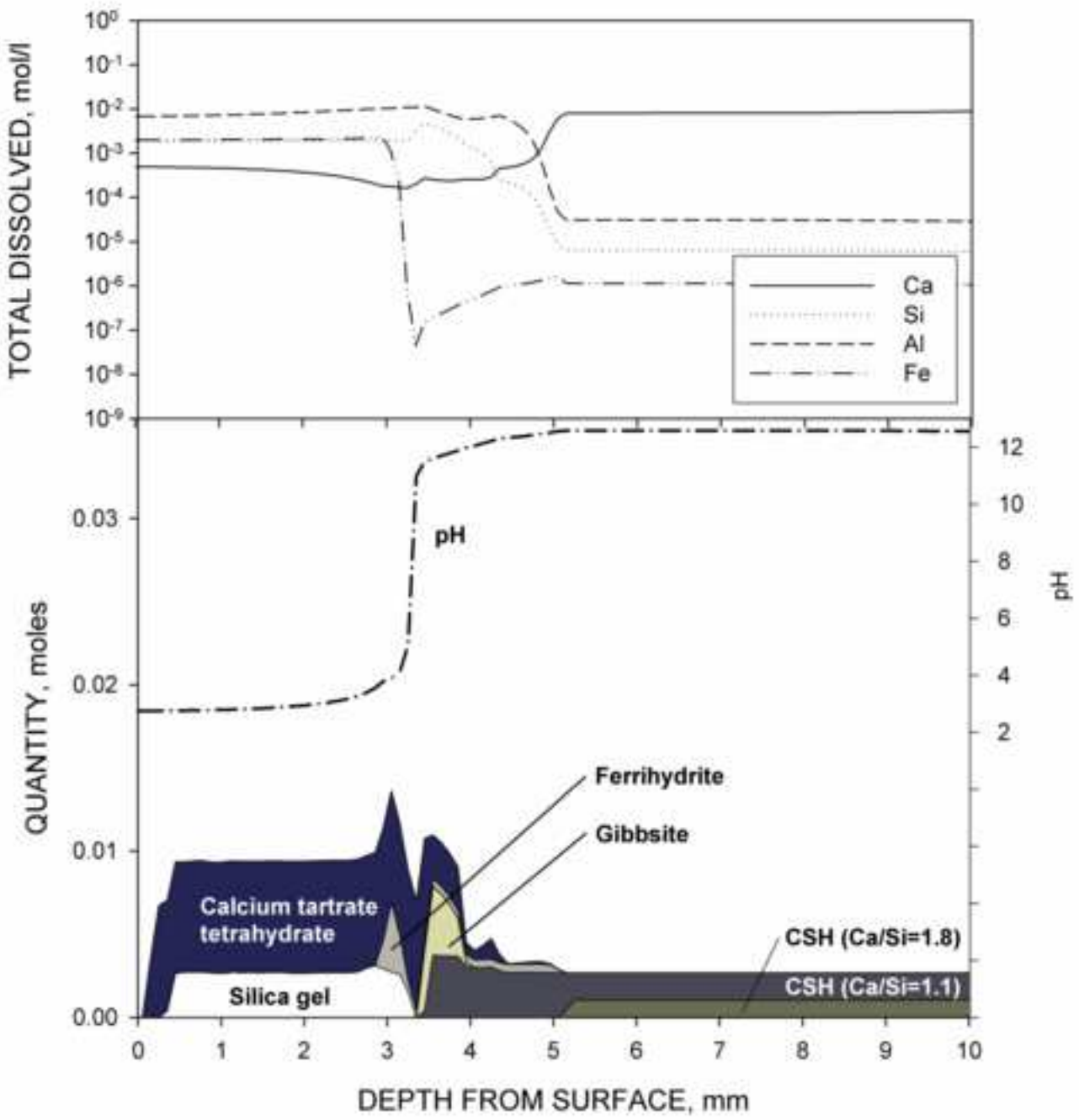

Figure 17

Click here to download Figure Figure 17.TIF

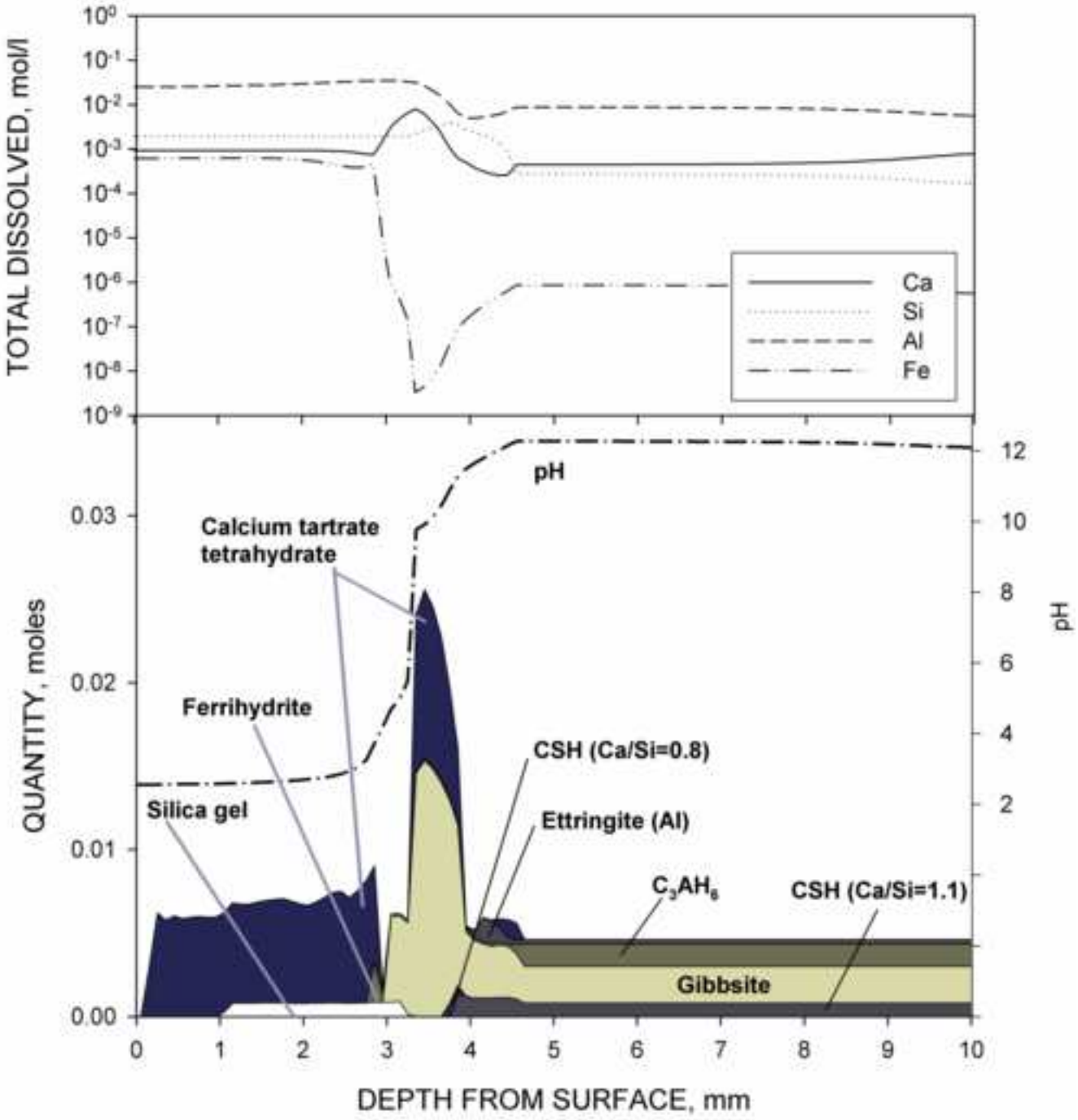

Figure 18

Click here to download Figure Figure 18.TIF

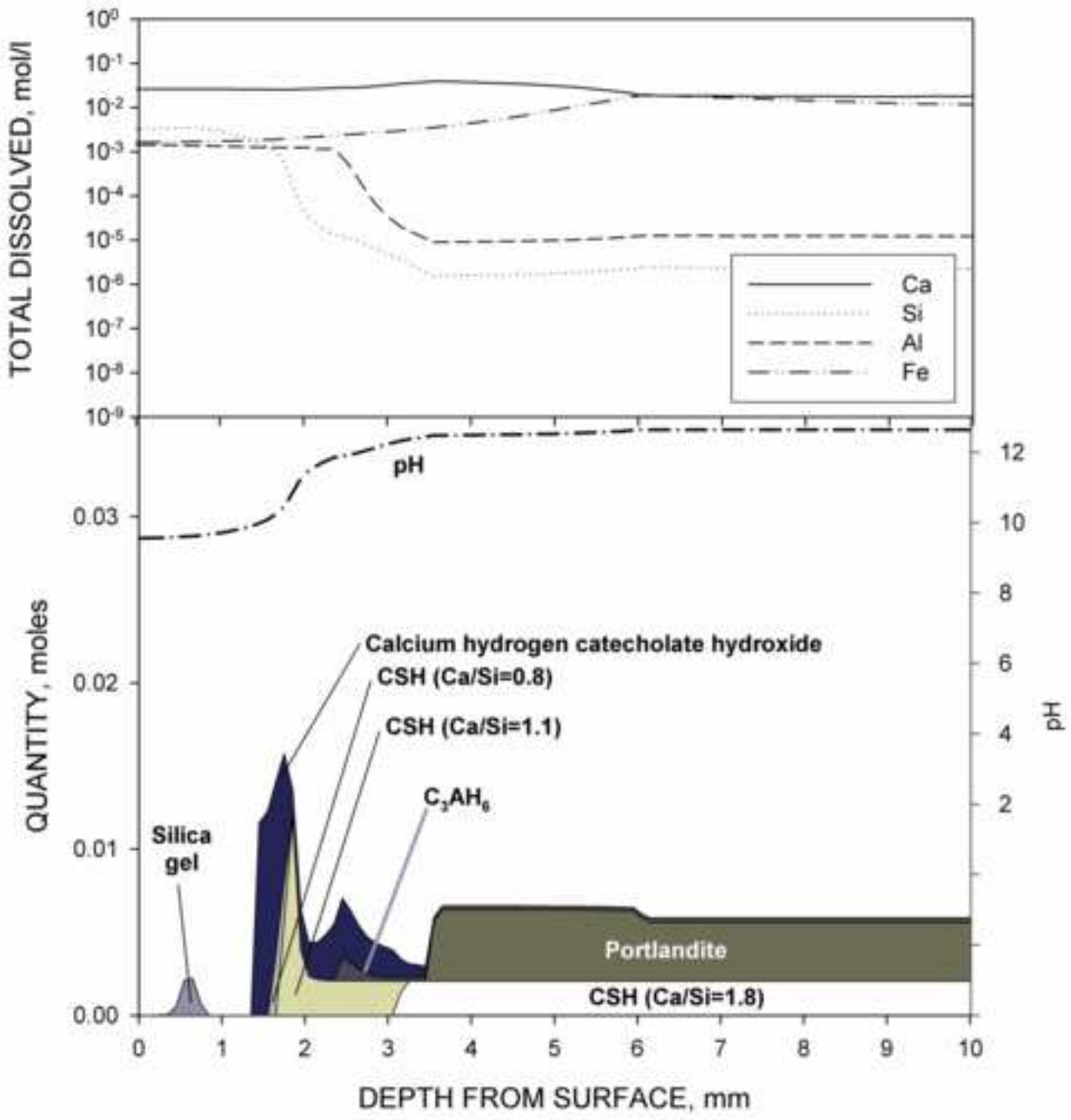

Figure 19

Click here to download Figure Figure 19.TIF

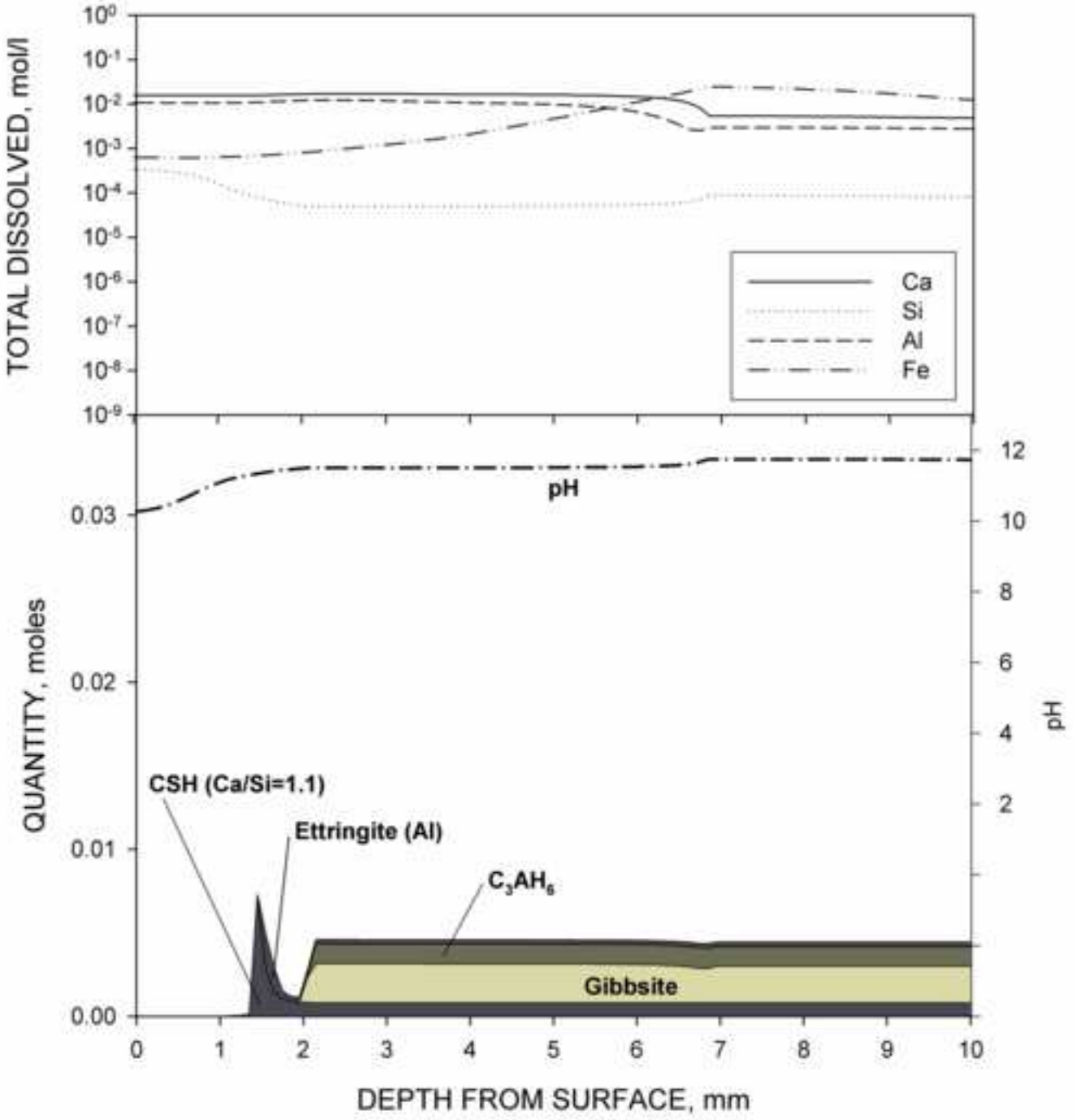

Table 1 Data relating to the organic acids studied.

ACID	FORMULA	ACID DISSOCIATION CONSTANT (pK_a)			REF.
		pK_{a1}	pK_{a2}	pK_{a3}	
Lactic acid	$C_3H_6O_3$	3.86			(Dawson, 1959)
		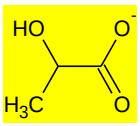 Lactate → 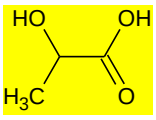 Lactic acid			
Citric acid	$C_6H_8O_7$	6.40	4.76	3.13	(Martell and Smith, 2004)
		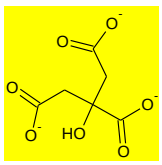 Citrate → 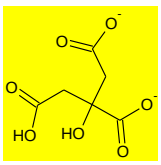 Hydrogen citrate → 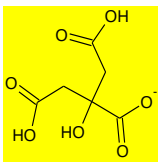 Dihydrogen citrate → 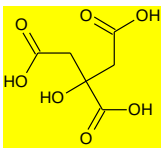 Citric acid			
Tartaric acid	$C_4H_6O_6$	6.40	2.70		(Martell and Smith, 2004)
		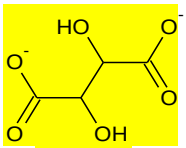 Tartrate → 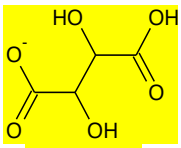 Hydrogen tartrate → 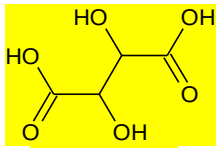 Tartaric acid			
Catechol	$C_6H_6O_2$	9.12	2.96		(Kortüm, Vogel and Andrussow, 1961)
		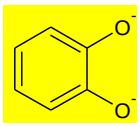 Catecholate → 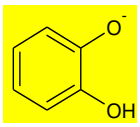 Hydrogen catecholate → 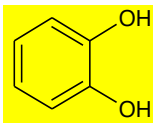 Catechol			

Table 2 Stability constants of complexes formed by calcium, aluminium and iron in water containing lactic acid.

COMPLEX	REACTION	STABILITY CONSTANT	REF.
Ca	$Ca^{2+} + C_3H_5O_3^- \rightleftharpoons Ca(C_3H_5O_3)^+$	0.90	(Martell and Smith, 2004)
	$Ca^{2+} + 2C_3H_5O_3^- \rightleftharpoons Ca(C_3H_5O_3)_2$	1.24	
Al	$Al^{3+} + C_3H_5O_3^- \rightleftharpoons Al(C_3H_5O_3)^{2+}$	1.21	(Marklund, Sjöberg, Öhman, Salvatore, Niinistö *et al*, 1986) (DL-Lactate)
	$Al^{3+} + 2C_3H_5O_3^- \rightleftharpoons Al(C_3H_5O_3)_2^+$	2.72	
	$Al^{3+} + 3C_3H_5O_3^- \rightleftharpoons Al(C_3H_5O_3)_3$	4.92	
	$Al^{3+} + 2\ C_3H_5O_3^- \rightleftharpoons Al(C_3H_4O_3)(C_3H_5O_3) + H^+$	6.17	

Table 3 Solubility and molar volume data for compounds relevant to the interaction of hydrated Portland cement with lactic acid.

COMPOUND	FORMULA / REACTION	SOLUBILITY PRODUCT, log K_{sp}	REF.	MOLAR VOLUME, cm^3/mol	REF.
Calcium lactate pentahydrate	$Ca(C_3H_5O_3)_2.5H_2O \rightleftharpoons Ca^{2+} + 2C_3H_5O_3^- + 5H_2O$	-0.97	(Apelblat, Manzurola, van Krieken and Nanninga, 2005)	unknown	(Bombi, Corain, Sheikh-Osman and Valle, 1990)
Aluminium lactate	$Al(C_3H_5O_3)_3 \rightleftharpoons Al^{3+} + 3C_3H_5O_3^-$	-0.45		212	
Ferrous lactate trihydrate	$Fe(C_3H_5O_3)_2.3H_2O \rightleftharpoons Fe^{2+} + 2C_3H_5O_3^- + 3H_2O$	-1.87		unknown	
Ferric lactate	$Fe(C_3H_5O_3)_3 \rightleftharpoons Fe^{3+} + 3C_3H_5O_3^-$	'soluble'	(Haynes, 2014)	unknown	

Table 4 Stability constants of complexes formed by calcium, aluminium and iron and silicon in water containing citric acid.

COMPLEX	REACTION	STABILITY CONSTANT	REF.
Ca	$Ca^{2+} + C_6H_5O_7^{3-} \rightleftharpoons Ca(C_6H_5O_7)^-$	4.87	(Martell and Smith, 2004)
	$Ca^{2+} + C_6H_5O_7^{3-} + H^+ \rightleftharpoons Ca(C_6H_6O_7)$	9.26	
	$Ca^{2+} + C_6H_5O_7^{3-} + 2H^+ \rightleftharpoons CaH(C_6H_7O_7)$	12.26	
Al	$Al^{3+} + C_6H_5O_7^{3-} \rightleftharpoons Al(C_6H_5O_7)$	9.97	
	$Al^{3+} + 2C_6H_5O_7^{3-} \rightleftharpoons Al(C_6H_5O_7)_2^{3-}$	14.80	
	$Al^{3+} + C_6H_5O_7^{3-} + H^+ \rightleftharpoons Al(C_6H_6O_7)^+$	12.85	
Fe (II)	$Fe^{2+} + C_6H_5O_7^{3-} \rightleftharpoons Fe(C_6H_5O_7^{3-})^-$	6.1	
	$Fe^{2+} + C_6H_5O_7^{3-} + H^+ \rightleftharpoons Fe(C_6H_6O_7^{3-})$	10.2	
Fe (III)	$Fe^{3+} + C_6H_5O_7^{3-} \rightleftharpoons Fe(C_6H_5O_7^{3-})$	13.1	
	$Fe^{3+} + C_6H_5O_7^{3-} + H^+ \rightleftharpoons Fe(C_6H_6O_7^{3-})^+$	14.4	
Si	$H_4SiO_4 + C_6H_5O_7^{3-} \rightleftharpoons Si(C_6H_5O_7)(OH)_4^{3-}$	0.11	(Öhman, Nordin, Sedeh and Sjöberg, 1991)

Table 5 Solubility and molar volume data for compounds relevant to the interaction of hydrated Portland cement with citric acid.

COMPOUND	FORMULA / REACTION	SOLUBILITY PRODUCT, log K_{sp}	REF.	MOLAR VOLUME, cm^3/mol	REF.
Calcium citrate tetrahydrate	$Ca_3(C_6H_5O_7)_2 \cdot 4H_2O \rightleftharpoons 3Ca^{2+} + 2C_6H_5O_7^{3-} + 4H_2O$	-14.94	(Goss, Lemons, Kerstetter and Bogner, 2007)	285*	(Herdtweck, Kornprobst, Sieber, Straver and Plank, 2011)
Calcium hydrogen citrate tetrahydrate	$Ca(C_6H_6O_7) \cdot 4H_2O \rightleftharpoons Ca^{2+} + C_6H_5O_7^{3-} + 4H_2O + H^+$	-0.33	(Seidell, 1919)	157	(Sheldrick, 1974)
Calcium dihydrogen citrate trihydrate	$Ca(C_6H_7O_7)_2 \cdot 3H_2O \rightleftharpoons Ca^{2+} + 2C_5H_5O_7^{3-} + 3H_2O + 4H^+$	0.77	(Seidell, 1919)	unknown	
Aluminium citrate	$Al(C_6H_5O_7) \rightleftharpoons Al^{3+} + C_6H_5O_7^{3-}$	1.26	(Froment, Buddington, Miller and Alfrey, 1989)	unknown	
Ferric citrate pentahydrate	$Fe(C_6H_5O_7).5H_2O \rightleftharpoons Fe^{3+} + C_6H_5O_7^{3-} + 5H_2O$	'slightly soluble' (-3.57)†	(Bertron and Duchesne, 2013)	unknown	

*Earlandite – may not be the same form of salt as that from which solubility data has been obtained.
†Value obtained using the midpoint of the solubility range ascribed to 'slightly soluble' (1 – 10 g/l).

Table 6. Stability constants of complexes formed by calcium, aluminium and iron in water containing D-tartaric acid.

COMPLEX	REACTION	STABILITY CONSTANT	REF.
Ca	$Ca^{2+} + C_4H_4O_6^{2-} \rightleftharpoons Ca(C_4H_4O_6)$	2.80	(Martell and Smith, 2004)
	$Ca^{2+} + C_4H_4O_6^{2-} + H^+ \rightleftharpoons Ca(C_4H_5O_6)^+$	5.86	
Al	$Al^{3+} + 2C_4H_4O_6^{2-} \rightleftharpoons Al(C_4H_4O_6)_2^-$	9.37	
Fe (II)	$Fe^{2+} + C_4H_4O_6^{2-} \rightleftharpoons Fe(C_4H_4O_6)$	3.10	
Fe (III)	$Fe^{3+} + C_4H_4O_6^{2-} \rightleftharpoons Fe(C_4H_4O_6)^+$	7.78	

Table 7. Solubility and molar volume data for compounds relevant to the interaction of hydrated Portland cement with tartaric acid.

COMPOUND	FORMULA / REACTION	SOLUBILITY PRODUCT, log K_{sp}	REF.	MOLAR VOLUME, cm^3/mol	REF.
Calcium tartrate tetrahydrate	$Ca(C_4H_4O_6)\cdot 4H_2O \rightleftharpoons Ca^{2+} + C_4H_4O_6^{2-} + 4H_2O$	-5.98	(Bertron and Duchesne, 2013)	141	(Hawthorn, Borys and Ferguson, 1982)
Calcium hydrogen tartrate	$Ca(C_4H_5O_6)_2 \rightleftharpoons Ca^{2+} + 2C_4H_4O_6^{2-} + 2H^+$	-7.55	(Seidell, 1919)	unknown	-
Dialuminium tritartrate	$Al_2(C_4H_4O_6)_3 \rightleftharpoons 2Al^{3+} + 3C_4H_4O_6^{2-}$	'Soluble'	(O'Neil, 2001)	unknown	-
Ferrous tartrate	$Fe(C_4H_4O_6)\cdot 2.5H_2O \rightleftharpoons Fe^{2+} + C_4H_4O_6^{2-} + 2.5H_2O$	-8.23	(Cayot, Guzun-Cojocaru and Cayot, 2013)	unknown	-
Ferric tartrate	$Fe_2(C_4H_4O_6)_3\cdot H_2O \rightleftharpoons 2Fe^{3+} + 3C_4H_4O_6^{2-} + H_2O$	-14.53*		unknown	-

*based on solubility data provided by a number of chemical suppliers, but original source unclear.

Table 8. Stability constants of complexes formed by aluminium and iron and silicon in water containing catechol.

COMPLEX	REACTION	STABILITY CONSTANT	REF.
Al	$Al^{3+} + C_6H_4O_2^{2-} \rightleftharpoons Al(C_6H_4O_2)^+$	6.34	(Öhman and Sjöberg, 1983)
	$Al^{3+} + 2C_6H_4O_2^{2-} \rightleftharpoons Al(C_6H_4O_2)_2^-$	15.44	
	$Al^{3+} + 3C_6H_4O_2^{2-} \rightleftharpoons Al(C_6H_4O_2)_3^{3-}$	28.62	
	$3Al^{3+} + 3C_6H_4O_2^{2-} + 3OH^- \rightleftharpoons Al_3(OH)_3(C_6H_4O_2)_3$	29.91	
	$Al^{3+} + 2C_6H_4O_2^{2-} + OH^- \rightleftharpoons Al(OH)(C_6H_4O_2)_2^{2-}$	23.45	
Fe (II)	$Fe^{2+} + C_6H_4O_2^{2-} \rightleftharpoons Fe(C_6H_4O_2)$	7.95	(Martell and Smith, 2004)
	$Fe^{2+} + 2C_6H_4O_2^{2-} \rightleftharpoons Fe(C_6H_4O_2)_2^{2-}$	13.5	
Fe (III)	$Fe^{3+} + C_6H_4O_2^{2-} \rightleftharpoons Fe(C_6H_4O_2)^+$	20.0	
	$Fe^{3+} + 2C_6H_4O_2^{2-} \rightleftharpoons Fe(C_6H_4O_2)_2^-$	34.7	
	$Fe^{3+} + 3C_6H_4O_2^{2-} \rightleftharpoons Fe(C_6H_4O_2)_3^{3-}$	43.8	
Si	$H_4SiO_4 + 3C_6H_6O_2 \rightleftharpoons Si(C_6H_4O_2)_3^{2-} + 2H^+ + 4H_2O$	-12.0	(Öhman, Nordin, Sedeh and Sjöberg, 1991)

Table 9. Solubility and molar volume data for compounds relevant to the interaction of hydrated Portland cement with catechol.

COMPOUND	FORMULA / REACTION	SOLUBILITY PRODUCT, log K_{sp}	REF.	MOLAR VOLUME, cm^3/mol	REF.
Calcium hydrogen catecholate hydroxide	$Ca(C_6H_5O_2)OH \rightleftharpoons Ca^{2+} + C_6H_4O_2^{2-} + H_2O$	-3.79	-*	755	(Dyer, 2011)
Calcium hydrogen catecholate catechol hydroxide	$Ca(C_6H_5O_2)(C_6H_6O_2)(OH).3H_2O \rightleftharpoons Ca^{2+} + 2C_6H_5O_2^{-} + 4H_2O$	-4.95	-*	903	

*Results of experiments used to obtain these values to be published in a forthcoming paper.

Table 10. Major oxide composition of the cements used in the study.

	% by mass		
CONSTITUENT	PC	PC/FA	CSA
CaO	67.80	47.17	44.38
SiO_2	20.67	28.94	10.71
Al_2O_3	4.16	9.44	31.75
Fe_2O_3	2.87	5.18	2.23
MgO	1.17	1.61	1.42
Na_2O	0.23	0.34	0.07
K_2O	0.61	1.07	0.28
TiO_2	0.41	0.60	1.47
MnO	0.05	0.06	0.02
P_2O_5	0.16	0.29	nd
SO_3	3.418	3.812	8.695
Cl	0.083	0.114	0.032

nd = not detected.

Table 11. Composition of the modelled mineral assemblages

	QUANTITY, moles		
PHASE	**PC**	**PC / FA**	**CSA**
Portlandite	5.79×10^{-3}	1.70×10^{-3}	-
CSH (Ca/Si = 0.8)	2.06×10^{-3}	2.69×10^{-3}	7.94×10^{-4}
Ettringite (Al)	9.04×10^{-9}	3.31×10^{-5}	1.93×10^{-4}
Ettringite (Fe)	1.82×10^{-5}	7.13×10^{-5}	6.59×10^{-5}
Monosulfate (Al)	1.29×10^{-4}	-	-
Monosulfate (Fe)	8.19×10^{-5}	-	-
C_2AH_8	1.51×10^{-4}	6.77×10^{-7}	1.86×10^{-3}
C_2FH_8	4.20×10^{-5}	1.65×10^{-4}	1.47×10^{-5}
C_3AH_6	2.91×10^{-5}	6.10×10^{-4}	-
Gibbsite	-	-	9.72×10^{-4}

Table 12

Table 12. Mineralogical analysis of the affected layer of cement paste specimens exposed to acid solutions estimated using Rietveld refinement of powder XRD traces.

	% by mass														
	Before exposure			Lactic			Citric			Tartaric			Catechol		
PHASE	PC	PC/FA	CSA	PC	PC/FA	CSA	PC	PC/FA	CSA	PC	PC/FA	CSA	PC	PC/FA	CSA
Portlandite	10.2	6.0	-	-	-	-			-	-	-	-	-	-	-
C_3S	1.7	0.8	-	-	-	-			-	-	-	-	-	-	-
C_2S	4.2	2.1	3.5	-	-	-			-	-	-	-	-	-	-
C_3A	-	-	0.6	-	-	-			-	-	-	-	-	-	-
Ye'elimite	-	-	0.4	-	-	-			-	-	-	-	-	-	-
Ettringite	1.8	1.6	3.1	-	-	-			-	-	-	-	-	-	-
Strätlingite	-	-	7.6	-	-	-			-	-	-	-	-	-	-
Quartz	-	-	-	-	4.3	-			-	-	1.1	-	0.5	3.1	-
Mullite	-	-	-	-	4.3	-			-	-	1.5	-	-	3.8	-
Hematite	-	-	-	-	0.5	-			-	-	0.2	-	-	0.4	-
Magnetite	-	-	-	-	0.5	-			-	-	0.2	-	-	0.4	-
Calcite	-	-	-	-	0.3	-	N/A	N/A	-	-	0.1	-	25.8	23.2	2.4
Gibbsite	-	-	0.9	-	-	28.3			21.0	-	-	23.9	-	-	20.6
Perovskite	-	-	1.0	-	-	4.1			8.0	-	-	5.9	-	-	3.5
Gehlenite	-	-	4.2	-	-	-			4.4	-	-	0.3	-	-	-
Calcium tartrate tetrahydrate	-	-	-	-	-	-			-	32.9	40.1	-	-	-	-
Hydroxysodalite-type phase	-	-	-	-	-	-			-	-	-	6.3	-	-	-
Thaumasite	-	-	-	-	-	-			-	-	-	-	2.3	-	-
Hemicarbonate	-	-	-	-	-	-			-	-	-	-	0.2	-	-
Monocarbonate	0.3	1.3	-	-	-	-			-	-	-	-	-	-	-
Monosulfate	0.6	8.2	-	-	-	-			-	-	-	-	-	-	8.2
Tartaric acid	-	-	-	-	-	-			-	-	0.6	-	-	-	
Amorphous	77.4	83.5	70.5	100.0	90.2	67.7			66.6	67.1	56.2	63.6	71.2	69.1	65.4

N/A = not available.

Table 13

Table 13. Chemical composition of the outer layers removed from the specimens after exposure to acid solutions.

	Lactic			Citric			Tartaric			Catechol		
	PC	PC/FA	CSA	PC	PC/FA	CSA	PC	PC/FA	CSA	PC	PC/FA	CSA
CaO	5.74	3.02	4.76	31.69	11.49	12.58	42.29	30.85	11.52	55.37	32.24	15.85
SiO_2	77.28	66.38	20.99	42.02	58.58	26.70	18.94	28.21	34.96	20.02	28.39	27.72
Al_2O_3	8.29	16.38	46.27	1.69	12.79	35.68	1.29	4.53	28.63	1.42	11.81	33.94
Fe_2O_3	1.87	6.43	3.71	1.10	4.43	3.74	1.61	3.66	3.08	1.01	5.52	2.40
MgO	0.69	0.91	1.15	0.30	0.60	0.83	0.07	0.21	0.76	1.86	2.98	1.86
Na_2O	0.05	0.49	0.00	0.09	0.00	0.03	0.04	0.15	0.00	0.05	0.38	0.17
K_2O	0.55	1.97	0.10	0.26	0.13	1.17	0.06	0.62	0.07	0.18	1.39	0.28
TiO_2	0.15	0.70	3.00	0.57	5.16	0.65	0.42	0.85	4.39	0.11	0.68	2.58
MnO	0.02	0.04	0.02	0.02	0.00	0.05	0.00	0.02	0.04	0.07	0.13	0.05
P_2O_5	0.26	0.29	0.32	0.00	0.00	0.23	0.09	0.09	0.11	0.66	0.72	0.43
SO_3^{2-}	0.06	0.18	0.58	0.00	0.14	0.63	0.05	0.08	0.45	1.44	0.68	0.48
Cl^-	0.01	0.06	0.015	0.00	0.00	0.00	0.01	0.01	0.02	0.02	0.01	0.27

Lactate molecule for Table 1

Click here to download Figure lactate.tif

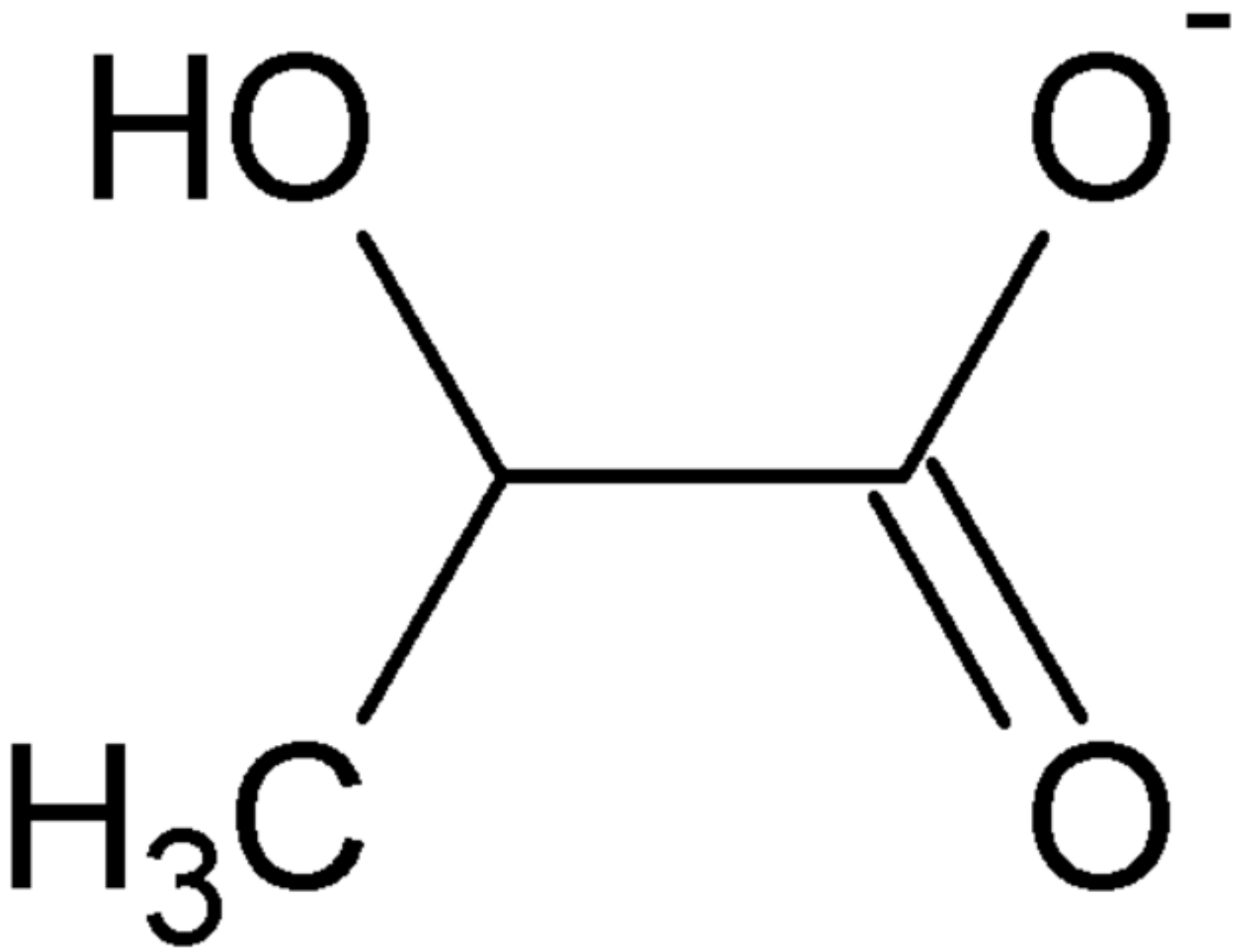

Lactic acid molecule for Table 1

Click here to download Figure lactic acid.tif

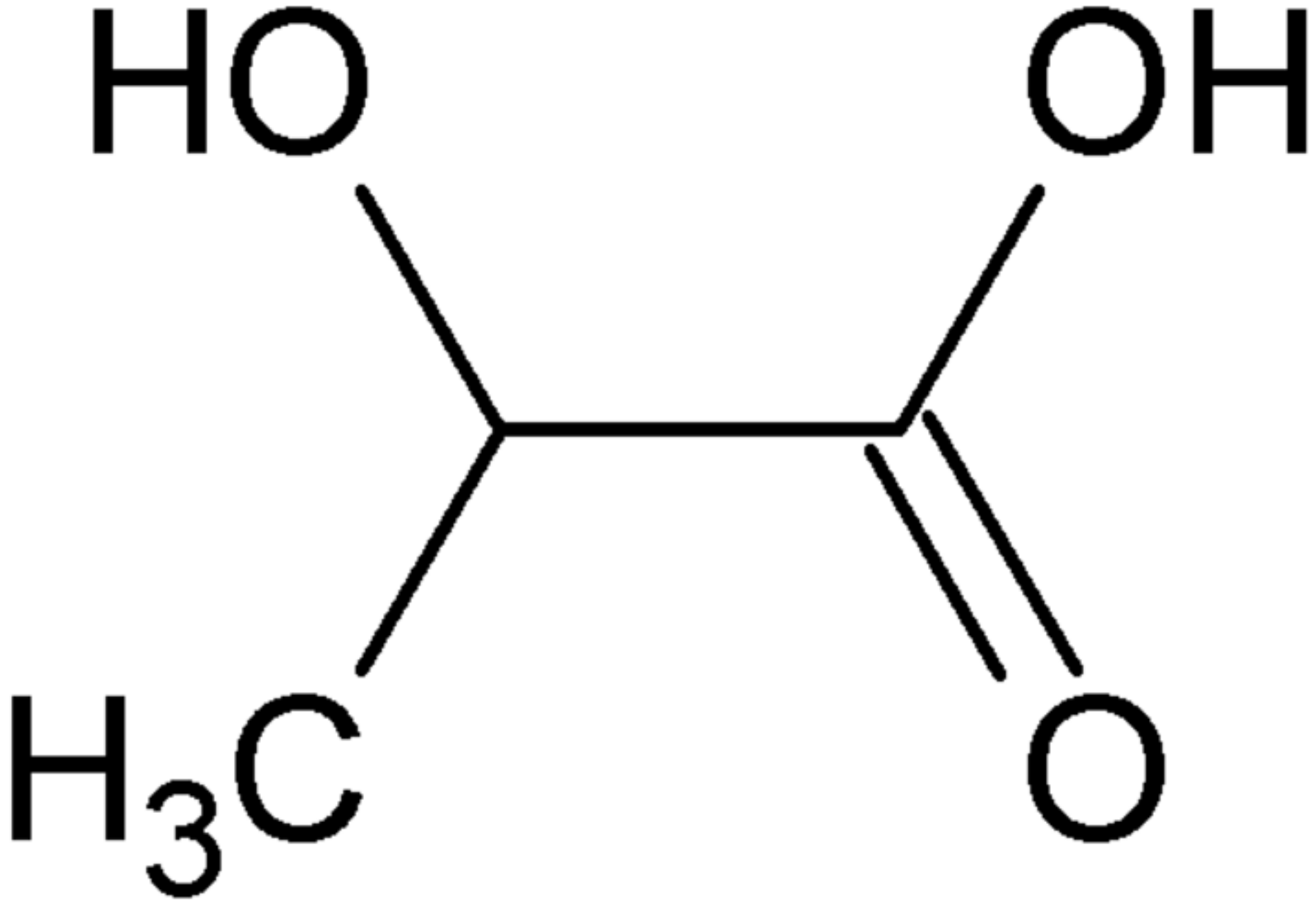

citrate molecule for Table 1

Click here to download Figure citrate.tif

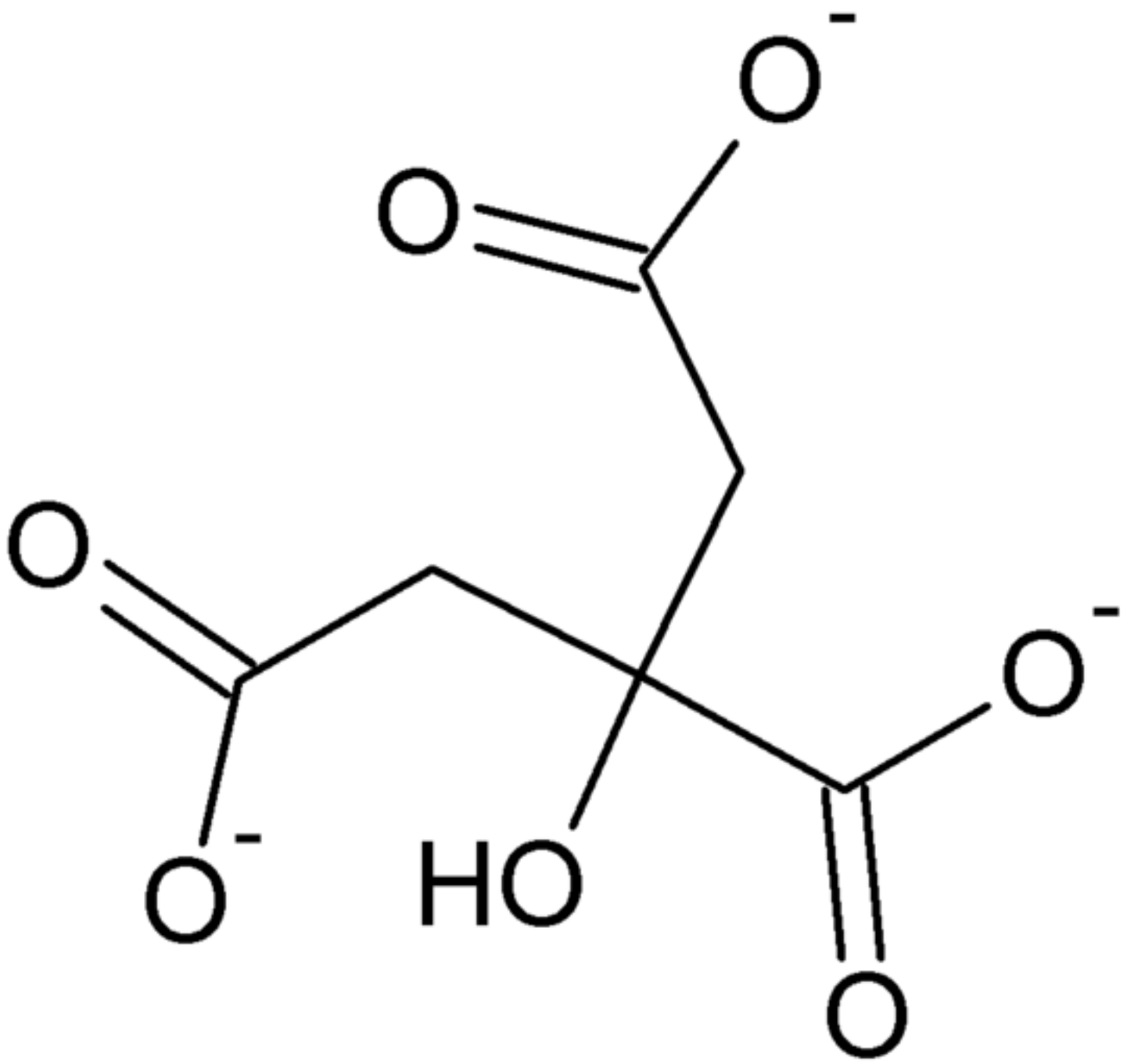

hydrogen citrate molecule for Table 1

Click here to download Figure hydrogen citrate.tif

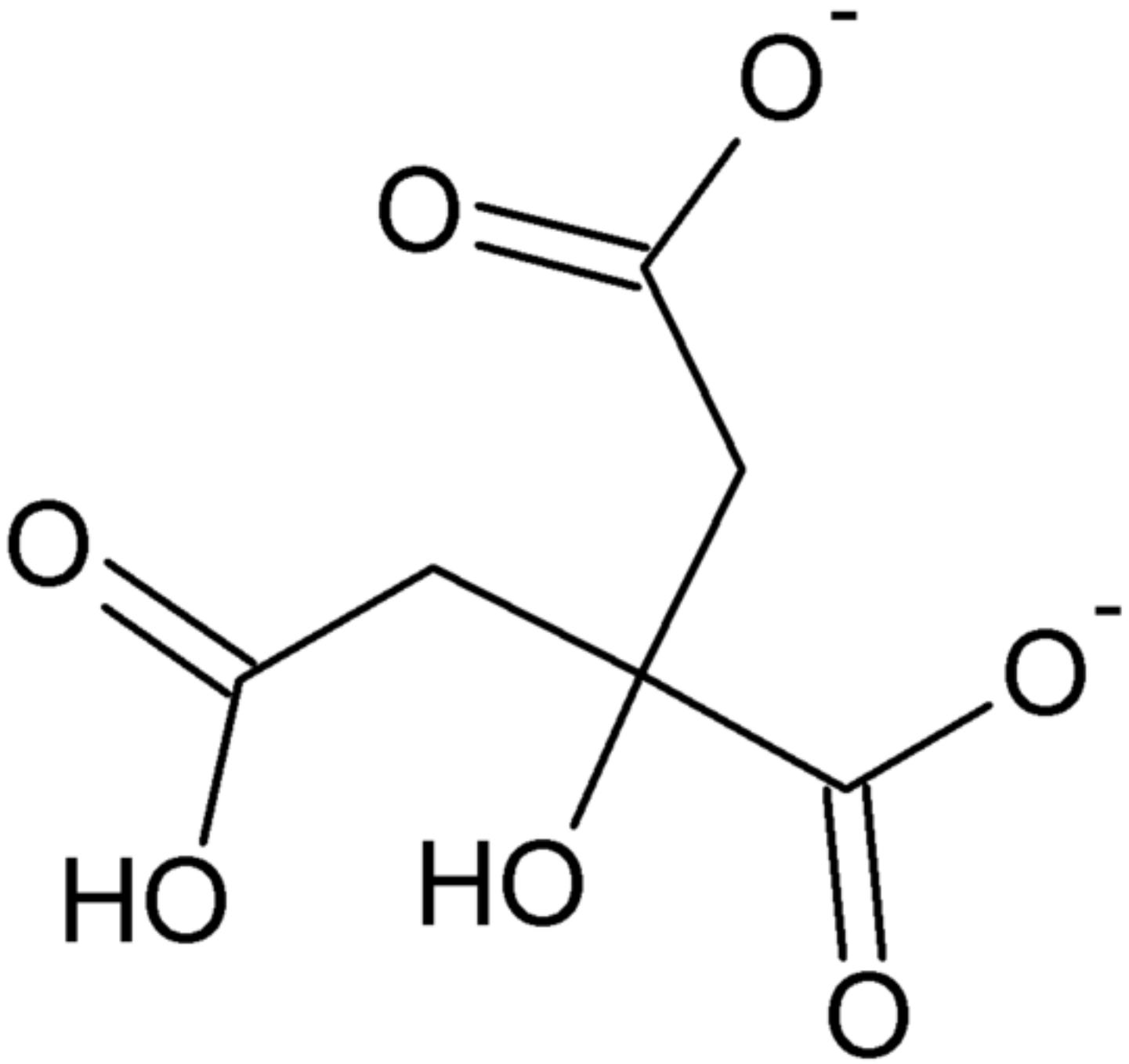

dihydrogen citrate molecule for Table 1

Click here to download Figure dihydrogen citrate.tif

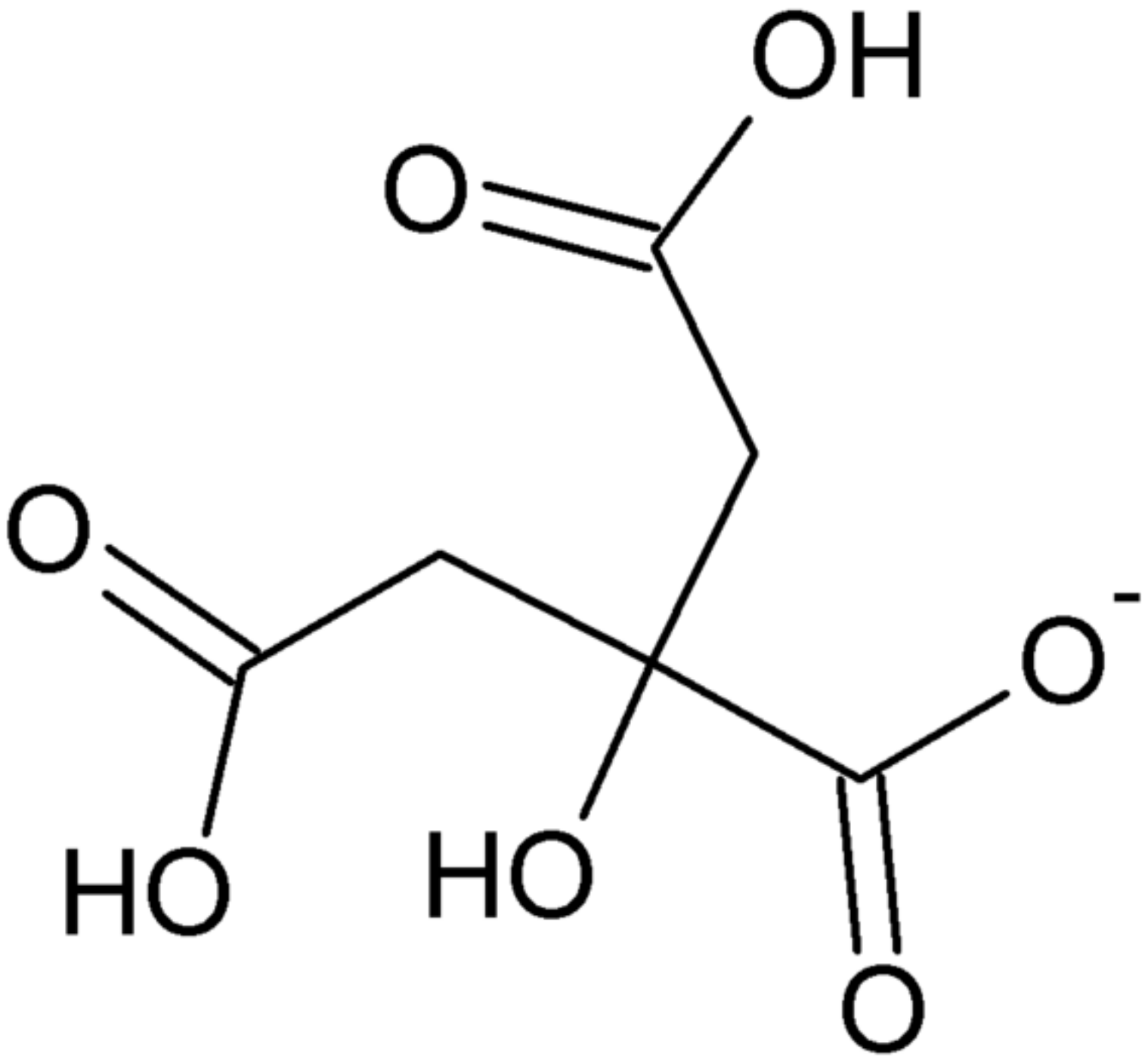

citric acid molecule for Table 1

Click here to download Figure citric acid.tif

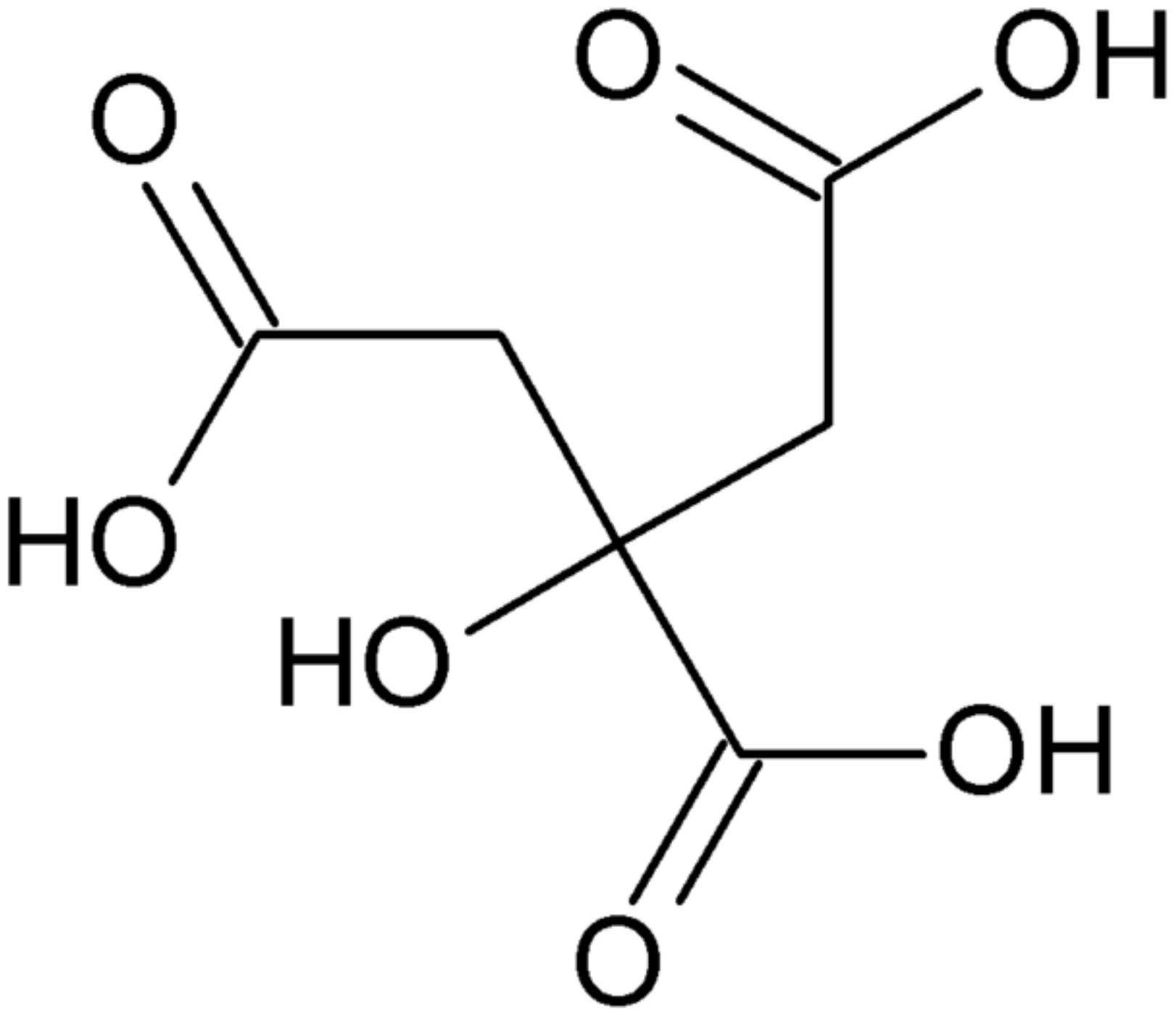

tartrate molecule for Table 1

Click here to download Figure tartrate.tif

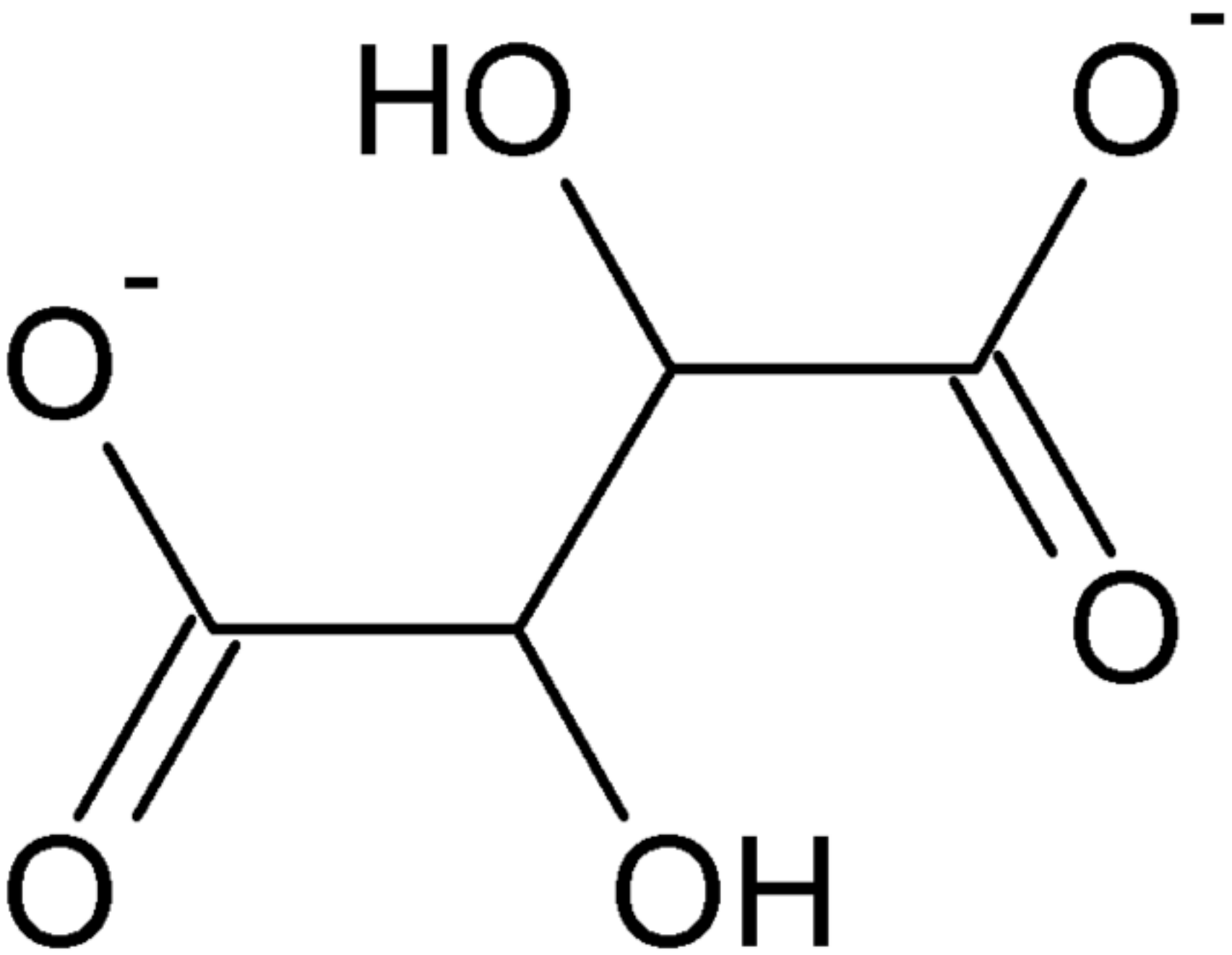

hydrogen tartrate molecule for Table 1

Click here to download Figure hydrogen tartrate.tif

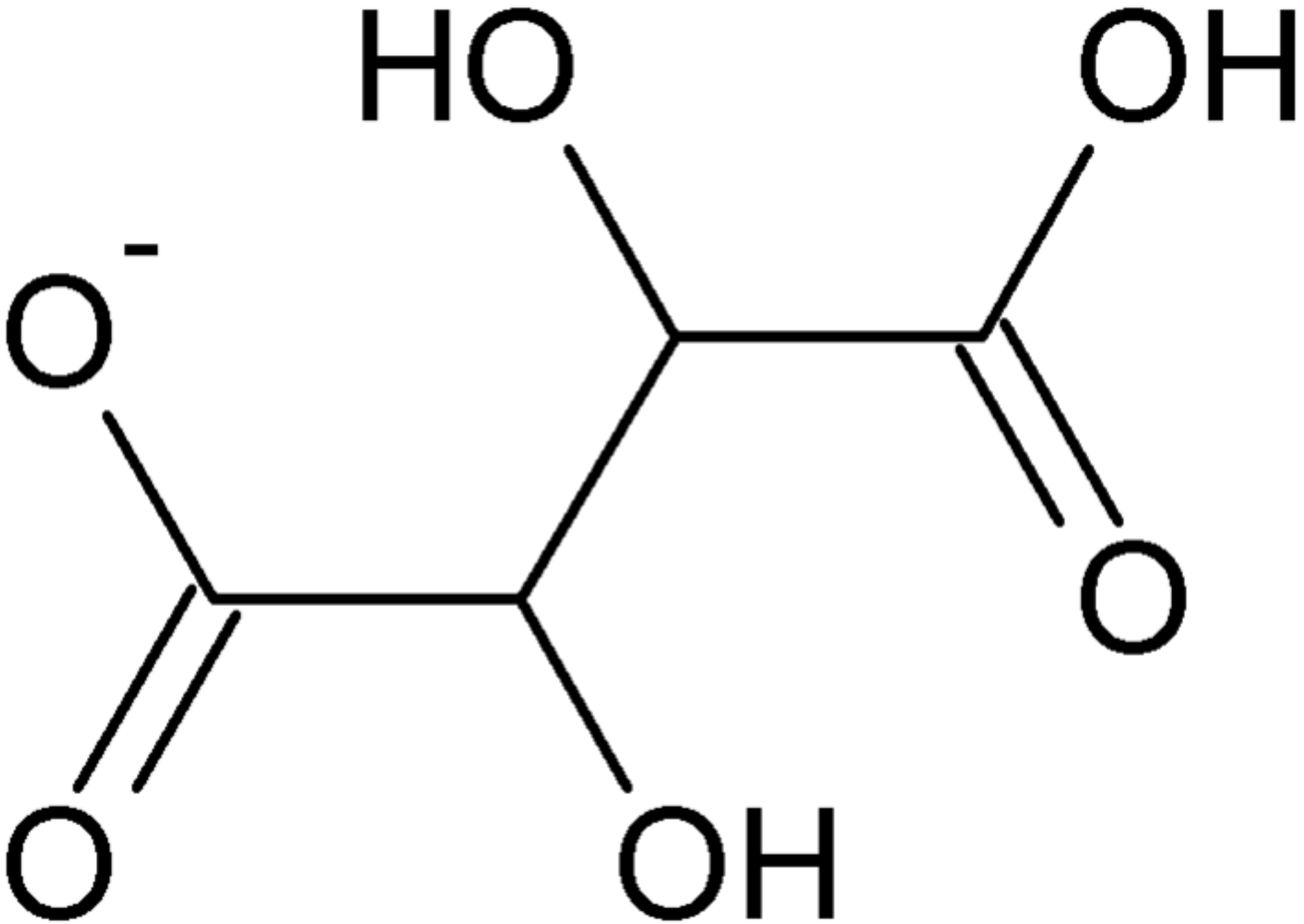

tartaric acid molecule for Table 1

Click here to download Figure tartaric acid.tif

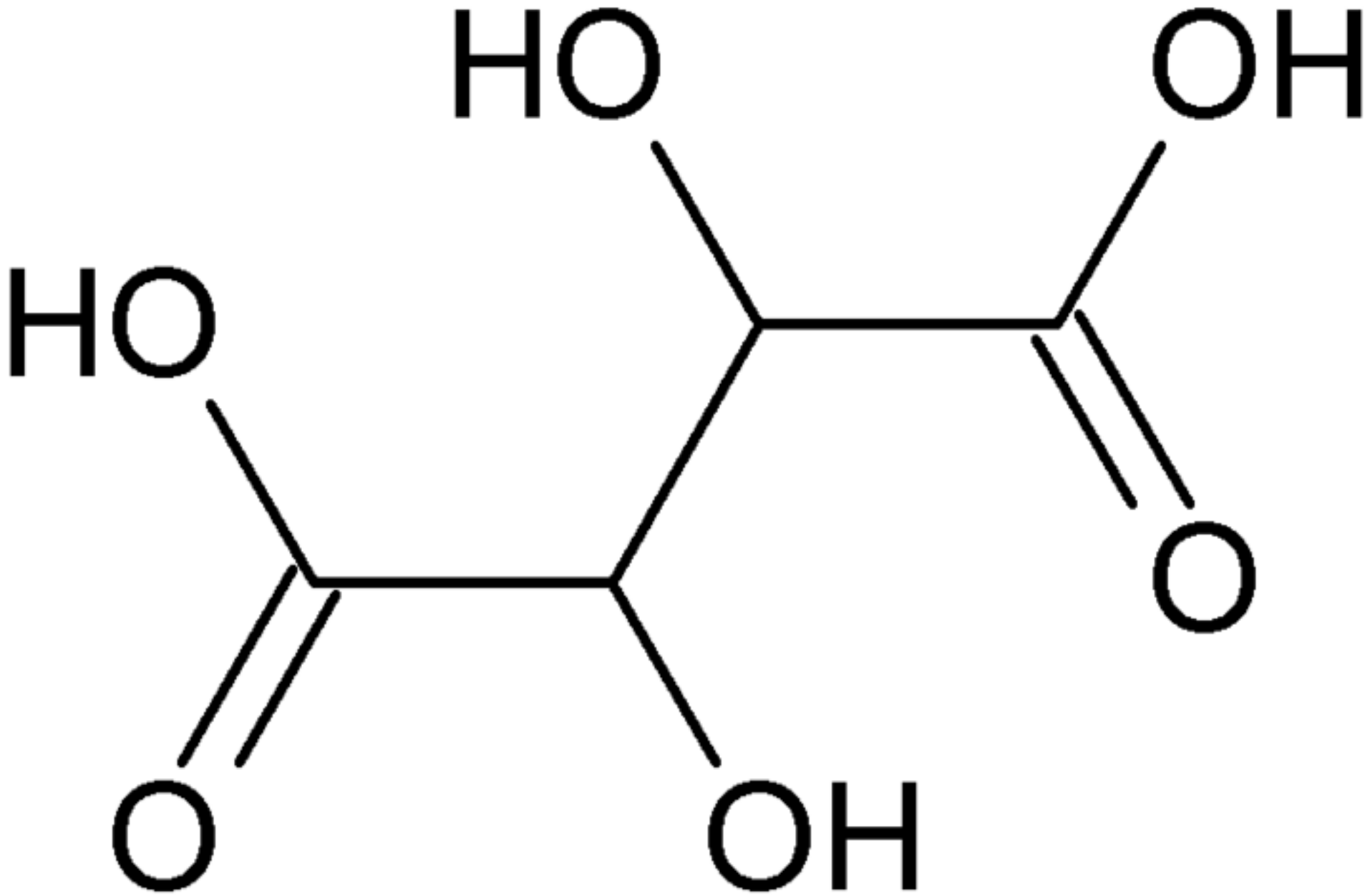

catecholate molecule for Table 1

Click here to download Figure catecholate.tif

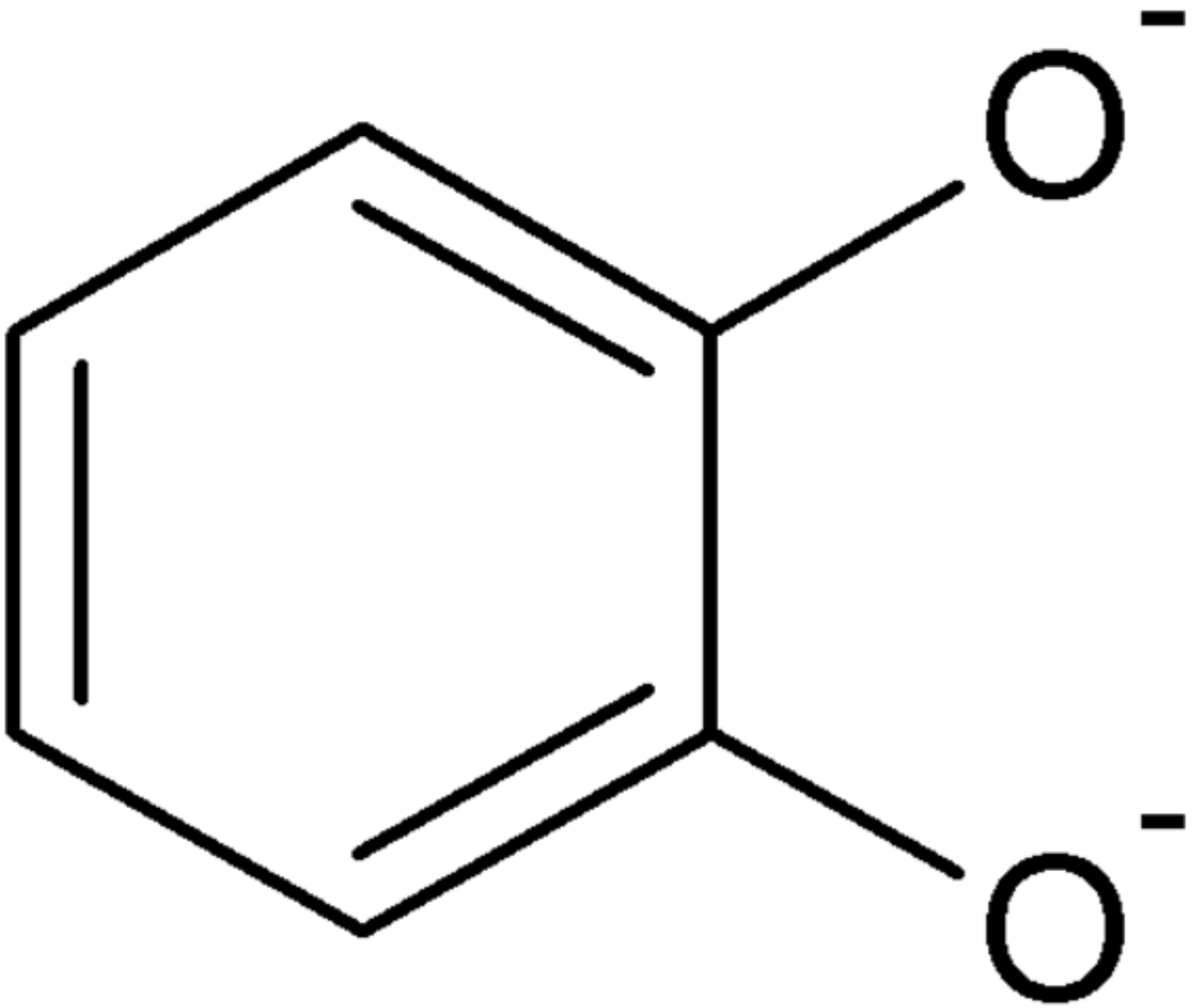

hydrogen catecholate molecule for Table 1

Click here to download Figure hydrogen catecholate.tif

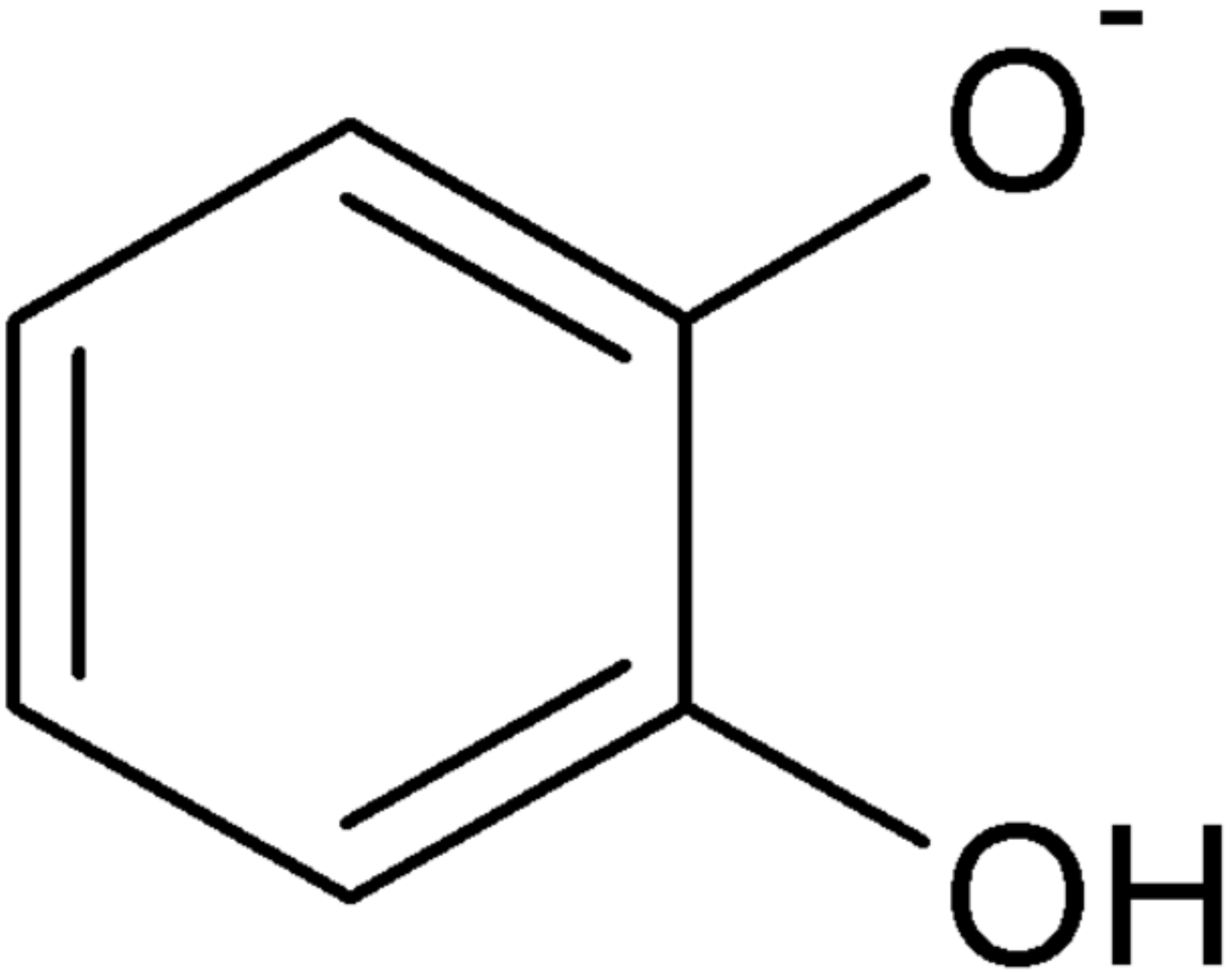

catechol molecule for Table 1

Click here to download Figure catechol.tif